Towards a Bulk Approach of Local Interactions of Hydrometeors

Manuel Baumgartner[1,2] and Peter Spichtinger[1]

[1]Institute for Atmospheric Physics, Johannes Gutenberg University, Johann-Joachim-Becher-Weg 21, 55128 Mainz, Germany
[2]Zentrum für Datenverarbeitung, Johannes Gutenberg University, Mainz, Germany

Correspondence to: Manuel Baumgartner (manuel.baumgartner@uni-mainz.de)

Abstract. Growth of small cloud droplets and ice crystals is dominated by diffusion of water vapor. Usually, Maxwell's approach of growth for isolated particles is used in describing this process. However, recent investigations show that local interactions between particles can change diffusion properties of cloud particles. In this study we develop an approach for including these local interactions into a bulk model approach. For this purpose, a simplified framework of local interaction is proposed and governing equations are derived from this setup. The new model is tested against direct simulations and incorporated into a parcel model framework. Using the parcel model, possible implications of the new model approach on clouds are investigated. The results indicate that for specific scenarios the lifetime of cloud droplets in subsaturated air may be longer, e.g. for an initially water supersaturated air parcel within a downdraft. These effects might have impact on mixed-phase clouds, e.g. in terms of riming efficiencies.

1 Introduction

Only recently, spatial distribution of hydrometeors, i.e. cloud droplets and ice crystals, has attained great attention in the context of small-scale turbulence in clouds. From idealized numerical simulations as well as experiments in cloud chambers one realized that hydrometeors may cluster in some regions of the clouds while other regions are relatively void (Shaw et al., 1998; Wood et al., 2005). Clustered hydrometeors influence each other in their diffusional growth by modifying the local field of supersaturation (see Castellano and Avila, 2011, for the case of droplet clusters). Although the existence of such clusters in real clouds remains quite controversial at the moment (Kostinski and Shaw, 2001; Vaillancourt and Yau, 2000; Devenish et al., 2012), it raises the question about their importance on the evolution of a whole cloud. The studies by Vaillancourt et al. (2001) and Vaillancourt et al. (2002) argue from direct numerical simulations, that local effects due to clustered cloud droplets in warm clouds may indeed modify diffusional growth of individual droplets but are not visible in the overall droplet spectrum. For typical turbulent situations occurring at cloud edge, Celani et al. (2005) and Celani et al. (2007) found much stronger influences of the local effects, although they probably excluded the mean growth of the droplets (Grabowski and Wang, 2013). However, the treatment of diffusional growth in all numerical cloud models relies on the diffusional growth theory developed by Maxwell and therefore assumes nearby hydrometeors not to affect each other regarding their diffusional growth behavior (see for example Rogers and Yau, 1989; Lamb and Verlinde, 2011; Wang, 2013; Maxwell, 1877).

In a mixed-phase cloud the picture may change dramatically since an ice crystal has a much more severe impact on the droplets in its vicinity: it may accelerate the evaporation of nearby droplets by growing at their expense. This local interaction
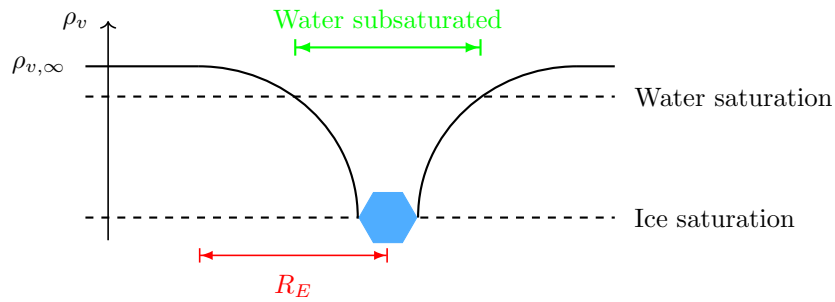
(a) Water supersaturated environment
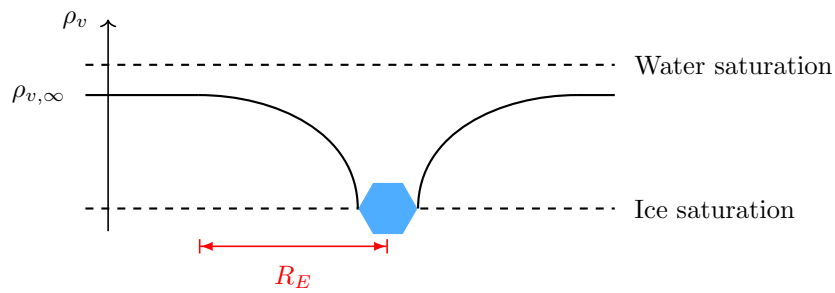
(b) Water subsaturated and ice supersaturated environment
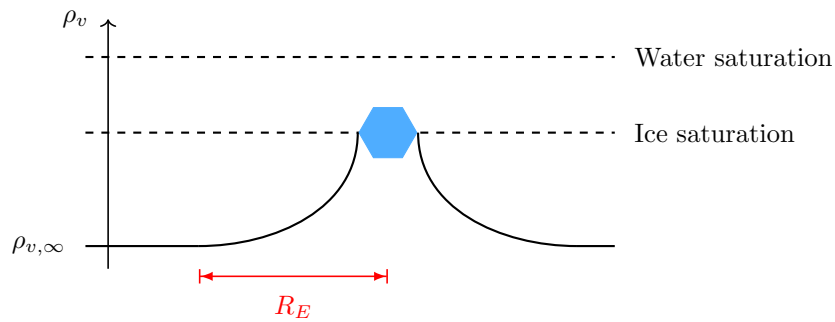
(c) Ice subsaturated environment

Figure 1. Schematic of the water vapor density field around an ice crystal with various environmental water vapor values $\rho_{v,\infty}$. Water vapor density at the ice crystal surface is assumed to equal the ice saturation density. In all cases, the ice crystal deforms the water vapor field locally within a ball of radius R_E. If a droplet has distance smaller than R_E from the ice crystal, its growth behavior is determined by the local value of water density instead of the environmental value $\rho_{v,\infty}$.

is not new and commonly referred to as the Wegener-Bergeron-Findeisen process (Wegener, 1911; Bergeron, 1949; Findeisen, 1938). Note that the Wegener-Bergeron-Findeisen process is different from the Ostwald ripening, where bigger particles grow at the expense of smaller particles due to the curvature dependency of the saturation pressure ("Gibbs-Thomson effect", see for example Lamb and Verlinde, 2011, chapter 3.4.1). Although the Wegener-Bergeron-Findeisen process is by definition a local process, numerical models do not represent it as such, since Maxwell's theory is applied and all hydrometeors grow according to the environmental rather than the local conditions. In Baumgartner and Spichtinger (2017b), we investigated the impacts of local interactions by diffusion between an ice crystal and surrounding droplets qualitatively using a reference model which resolves the hydrometeors as well as the vapor and temperature fields. For convenience, we put the results from Baumgartner and Spichtinger (2017b) into a "guiding schematic", illustrating the local water vapor field configurations, see figure 1. If a droplet has distance smaller than R_E from the ice crystal, only the local value of water vapor density is seen by the droplet and therefore dictates its diffusional growth behavior. If the local droplet number is high enough, they influence the ice crystal and may even disconnect its growth behavior from the environmental conditions. In both cases, Maxwellian growth theory is not applicable. Apart from numerical simulations, the question of solvability of the underlying governing equations is addressed in Baumgartner and Spichtinger (2017a); for a reduced model problem existence and uniqueness of solutions could be proven.

In this study, we focus on a theoretical description of local interactions between an ice crystal and nearby droplets suited to be incorporated into a bulk-microphysical formulation. This study is organized as follows: section 2 contains a derivation and a discussion of the model equations. In section 3 we describe the incorporation of the new model into a simple parcel model in order to assess possible implications on a whole cloud. Finally we end with a summary and concluding remarks in section 4.

2 Derivation of the Model Equations

This section is dedicated to the description and derivation of the model equations describing local interactions between an ice particle and surrounding cloud droplets. Subsection 2.1 contains the derivation. We comment on the choice of the involved parameters in subsection 2.2 and afterwards present a model simplification in subsection 2.3 while subsection 2.4 contains a general discussion of the suggested model equations.

2.1 Local Ice-Droplet System

2.1.1 Description

As a conceptual model for a local configuration of an ice crystal and a droplet, we consider the schematic shown in figure 2. A spherical ice crystal with radius R_i is located in the center. Water vapor density and temperature at the surface of the ice crystal are denoted by $\rho_{v,i}, T_i$, respectively. A droplet with radius r_d is located at distance R_* from the ice crystal center. We henceforth call R_* the "coupling distance" of the ice crystal–droplet interaction. Let $\rho_{v,d}, T_d$ denote water vapor density and temperature at the surface of the droplet, respectively. Radius R_E denotes the "radius of influence" of the ice crystal, defined as the radius, where the ice crystal deforms the surrounding fields of water vapor and temperature in a non-negligible manner.
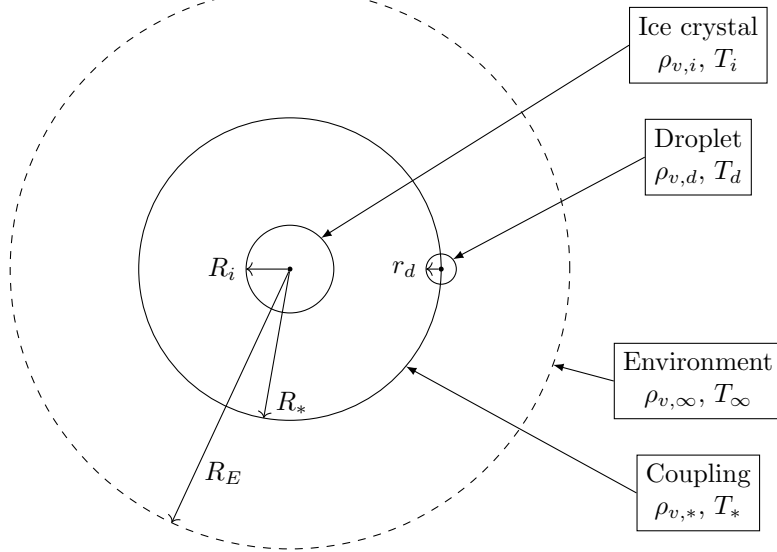
Figure 2. Conceptual model of local ice-droplet system. In the center is an ice crystal with radius R_i and at distance R_* from the ice crystal is a cloud droplet with radius r_d. The presence of the ice crystal gives rise to an influence sphere with radius R_E around the ice crystal. Distance R_* is the coupling distance, where the diffusional growth of the hydrometeors is coupled.

We will discuss a possible choice of the radius of influence in section 2.2.2, where we regard the vapour field as deformed in a non-negligible manner, if the relative deviation of the local value and the ambient value exceeds $0.1\,\%$. The radius of influence gives rise to a "sphere of influence" around the ice crystal, wherein its influence on the fields for water vapor and temperature cannot be ignored. The values for water vapor density and temperature at the boundary of the influence sphere around the ice crystal are given by the environmental values $\rho_{v,\infty}$ and T_∞. The corresponding values at coupling distance R_* are denoted by $\rho_{v,*}$ and T_*. We will describe the local coupling of both hydrometeors with the help of the values $\rho_{v,*}, T_*$, so we call them the "coupling values". Within this study, we denote variables referring to properties of the ice crystal with uppercase letters and variables referring to the droplet with lowercase letters.

In this study, we assume always spherical shape of the ice crystals and a negligible relative sedimentation velocity between the ice crystal and the neighboring droplet. Both assumptions are modelling assumptions. The assumption of a spherical ice crystal influences the growth behaviour of the ice crystal as well as the growth behaviour of the surrounding droplet, see appendix A for an example. Including the effect of ice crystal shape on the diffusional growth of the surrounding droplet is beyond the scope of this study and would require precise informations about the position of the droplet relative to the ice crystal, which is not available in models. In order to include the effect of the ice crystal shape on its own growth by diffusion, we could replace the growth equation (5a) by a variant using the ice crystal capacity (Lamb and Verlinde, 2011, Chapter 8.3.1). Moreover, we could also replace the Maxwellian growth equation for the ice crystal by the model given in Chen and Lamb (1994) to model changes in ice crystal shape. Both modifications could improve the representation of the ice crystal growth,

but also lead to an inconsistency in the model because in the following we need the assumption of spherical symmetricity. Therefore we stick to the simpler growth equations.

As mentioned above, we consider water vapor and temperature fields as spherically symmetric inside the influence sphere as is done in Maxwellian growth theory. This assumption is not fully consistent with the schematic in figure 2, since spherical symmetry is not able to account for a spatial localized droplet as depicted in the schematic. Assuming spherical symmetric fields means that the droplet is replaced by a continuous source or sink for water vapor and temperature along the sphere with radius R_*. This point of view also allows the generalization to the case of multiple droplets by appropriately changing the strength of the source or the sink.

As was done for the ice crystal, we may analogously define a sphere of influence for the droplet with corresponding radius of influence r_E. In order to use Maxwellian growth theory to describe droplet growth, we have to specify the values for water vapor density and temperature at the radius of influence r_E. We will use the coupling values $\rho_{v,*}$ and T_* as the environmental values in the droplet growth equation, i.e. as the values at the radius of influence r_E. With this choice, droplet growth responds to the coupling values.

The idea of the model is as follows. The ice crystal first establishes fields for water vapor and temperature as if it were isolated, yielding values at the coupling distance R_*. These fields are given by the equilibrium fields for water vapor and temperature around the ice crystal and serve as background fields, see equation (1). Since the droplet is located at coupling distance R_*, the coupling values $\rho_{v,*}, T_*$ define the ambient values for its diffusional growth. We establish an equation for the coupling values (see equations (7) and (6)), causing the droplet to grow or evaporate. This growth or evaporation feeds back to the coupling values and will in turn influence the growth behavior of the ice crystal.

In the following, we will derive the model equations, resulting finally in the ODE system (19), consisting of the growth equations for the ice crystal (equations (19a) and (19b)), the growth equations of the droplet (equations (19c) and (19d)) and the evolution equations for the coupling values (equations (19e) and (19f)).

2.1.2 Derivation

The spherical symmetric solutions of the Laplace equations $\Delta \rho_v = 0$ and $\Delta T = 0$ for ρ_v and T inside the influence sphere of the ice crystal, describing the water vapor density and temperature field, are given by

$$\rho_v(R) = \frac{\rho_{v,\infty} R_E - \rho_{v,i} R_i}{R_E - R_i} + \frac{(\rho_{v,i} - \rho_{v,\infty}) R_i R_E}{R_E - R_i} \frac{1}{R}, \tag{1a}$$

$$T(R) = \frac{T_\infty R_E - T_i R_i}{R_E - R_i} + \frac{(T_i - T_\infty) R_i R_E}{R_E - R_i} \frac{1}{R} \tag{1b}$$

where R is the radial distance from the ice crystal center. Equations (1) define the unperturbed background fields for an isolated ice crystal, representing the spatial thermodynamic equilibrium. The corresponding solutions inside the influence sphere of the

droplet are

$$\widehat{\rho_v}(r) = \frac{\rho_{v,*}r_E - \rho_{v,d}r_d}{r_E - r_d} + \frac{(\rho_{v,d} - \rho_{v,*})r_E r_d}{r_E - r_d}\frac{1}{r}, \tag{2a}$$

$$\widehat{T}(r) = \frac{T_* r_E - T_d r_d}{r_E - r_d} + \frac{(T_d - T_*)r_E r_d}{r_E - r_d}\frac{1}{r} \tag{2b}$$

where r is the radial distance from the droplet center. Proceeding as in the derivation of the Maxwellian growth equations, we

5   obtain from (2) the following equations for the change in droplet mass and temperature

$$\frac{\mathrm{d}m_d}{\mathrm{d}t} = 4\pi\alpha_d D_0 r_d r_E \frac{\rho_{v,*} - \rho_{v,d}}{r_E - r_d}, \tag{3a}$$

$$\frac{\mathrm{d}T_d}{\mathrm{d}t} = \frac{4\pi r_d r_E}{m_d c_{p,l}(T_d)(r_E - r_d)}\Big(L_{lv}(T_d)\alpha_d D_0(\rho_{v,*} - \rho_{v,d}) + K_0(T_* - T_d)\Big), \tag{3b}$$

where m_d denotes the droplet mass, T_d the droplet temperature, α_d the accommodation coefficient (Davis, 2006), D_0 the diffusivity of air, K_0 the thermal conductivity of air, $c_{p,l}$ the specific heat capacity of liquid water and L_{lv} the latent heat of

10   vaporization. Using representation (2) of the water vapor field, the rate J_d of water vapor exchange through the ball b_E with radius r_E around the droplet is given by

$$J_d = -\int_{\partial b_E} D_0 \nabla\widehat{\rho_v}\cdot N\,\mathrm{d}\sigma = -D_0\frac{\rho_{v,*} - \rho_{v,d}}{r_E - r_d}\frac{r_d}{r_E}4\pi r_E^2 = -\frac{1}{\alpha_d}\frac{\mathrm{d}m_d}{\mathrm{d}t} \tag{4}$$

where N denotes the outer normal vector at the surface ∂b_E.

The growth equations for the ice crystal are given by

$$\frac{\mathrm{d}M_i}{\mathrm{d}t} = 4\pi\alpha_i D_0 R_i R_* \frac{\rho_{v,*} - \rho_{v,i}}{R_* - R_i}, \tag{5a}$$

$$\frac{\mathrm{d}T_i}{\mathrm{d}t} = \frac{4\pi R_i R_*}{M_i c_{p,i}(T_i)(R_* - R_i)}\Big(\alpha_i D_0 L_{iv}(T_i)(\rho_{v,*} - \rho_{v,i}) + K_0(T_* - T_i)\Big) \tag{5b}$$

where M_i denotes the ice crystal mass, T_i the ice crystal temperature, α_i the accommodation coefficient, $c_{p,i}$ the specific heat of ice and L_{iv} the latent heat for sublimation. Note that in equations (3) and (5) the coupling values $\rho_{v,*}, T_*$ show up to allow the coupling of the diffusional growth of the hydrometeors.

20   After the description of the respective growth equations, we proceed to the coupling values. We define

$$T_*(t) := T(R_*) \quad \text{and consequently} \quad \frac{\mathrm{d}T_*}{\mathrm{d}t} = \frac{\mathrm{d}}{\mathrm{d}t}\Big(T(R_*)\Big), \tag{6}$$

with T being the unperturbed background temperature field of the ice crystal from equation (1). As in Maxwellian growth theory, in definition (6) we assume temperature fluctuations to balance quickly and not to affect the droplet growth. We define the evolution equation for the coupling value $\rho_{v,*}$ as

$$\frac{\mathrm{d}\rho_{v,*}}{\mathrm{d}t} := I_1 + I_2 + I_3 \tag{7}$$

being the sum of three terms I_1, I_2, I_3, representing three different physical processes:
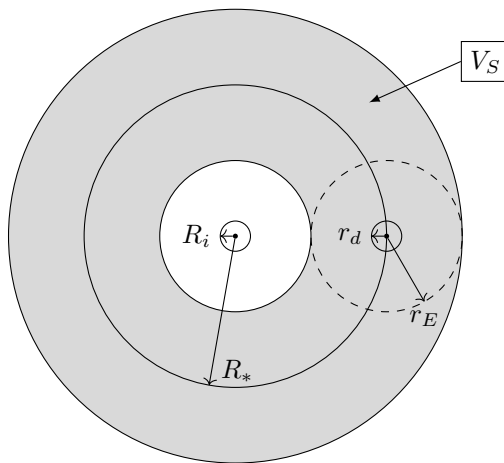
Figure 3. Illustration of the spherical shell, obtained by extending the surface of the sphere with interaction radius R_* around the ice crystal. Within the gray shaded area, representing the volume V_S of the spherical shell, we assume a uniform distribution of water vapor and temperature.

- I_1 models the time evolution of the unperturbed water vapor field of the ice crystal,

- I_2 takes the influence of the droplet on the coupling water vapor density into account,

- I_3 describes the relaxation of the coupling value back to the value of the thermodynamic equilibrium $\rho_v(R_*)$.

The first term I_1 takes the unperturbed background value $\rho_v(R_*)$ of an isolated ice crystal into account. As rate of change for this value, we define

$$I_1 := \frac{\mathrm{d}}{\mathrm{d}t}\left(\rho_v(R_*)\right). \tag{8}$$

If no droplet is present, we will have $I_2 = I_3 = 0$ in equation (7) and definition (8) simply ensures $\rho_{v,*}$ to equal the background value $\rho_v(R_*)$.

The second term I_2 considers the change of water vapor density due to droplet growth or evaporation. The rate of water vapor exchange J_d of the droplet is given in equation (4). The released water vapor is assumed to diffuse in unit time into some volume V, to be defined later, leading to the water vapor exchange rate $\frac{J_d}{V}$. Due to the assumed spherical symmetry, using the exchange rate $\frac{J_d}{V}$ directly amounts to assuming the sphere with radius R_* around the ice crystal as being filled up with droplets and their influence spheres, resulting in a strong overestimation of the droplet effect, so we have to rescale this rate. Assume the sphere with radius R_* around the ice crystal as being extended to a spherical shell with thickness $2r_E$ as in figure 3. This spherical shell is only introduced for the derivation of the coupling density equation (7). The value

$$Z := \frac{\frac{4}{3}\pi\left((R_* + r_E)^3 - (R_* - r_E)^3\right)}{\frac{4}{3}\pi r_E^3} = \frac{(R_* + r_E)^3 - (R_* - r_E)^3}{r_E^3} \tag{9}$$

measures the number of droplet influence spheres fitting inside the spherical shell. We take this value of Z to rescale the exchange rate and define the new value of I_2 as $\frac{J_d}{ZV}$. In reality, influence spheres of droplets may also overlap, leading to another local competition for water vapor between the droplets and a larger value for Z. However, our choice assumes a local well-mixed droplet distribution around the ice crystal and we neglect a possible local competition between the droplets. If we consider not only a single droplet but in total N_d droplets inside the influence sphere of the ice crystal, we finally define the exchange rate as

$$I_2 := N_d \frac{J_d}{ZV} = -\frac{N_d}{\alpha_d ZV} \frac{\mathrm{d}m_d}{\mathrm{d}t}, \tag{10}$$

where we used equation (4). This rate actually neglects local interactions and competitions between the droplets inside the influence sphere of the ice crystal and assumes all droplets as identical.

Finally, the third term I_3 accounts for the relaxation of the coupling value for water vapor density $\rho_{v,*}$ to $\rho_v(R_*)$, provided by the background field and representing thermodynamic equilibrium. Motivated by Fick's law of diffusion, let

$$-\int_{\partial B_*} D_0 \frac{\rho_{v,*} - \rho_v(R_*)}{R_E - R_*} \,\mathrm{d}\sigma = -4\pi R_*^2 D_0 \frac{\rho_{v,*} - \rho_v(R_*)}{R_E - R_*} \tag{11}$$

be the rate of water vapor exchange from ball B_* to the outside, where B_* denotes the ball with coupling radius R_* around the ice crystal. The change of the coupling vapor density is therefore given by

$$I_3 := -\int_{\partial B_*} D_0 \frac{\rho_{v,*} - \rho_v(R_*)}{R_E - R_*} \,\mathrm{d}\sigma \frac{1}{\frac{4}{3}\pi R_*^3} = -3D_0 \frac{1}{R_*} \frac{\rho_{v,*} - \rho_v(R_*)}{R_E - R_*}. \tag{12}$$

Definition (12) represents a possible choice for the relaxation rate, but should ideally be reviewed with the help of measurements.

Altogether, substituting equations (8), (10) and (12) into (7) yields

$$\frac{\mathrm{d}\rho_{v,*}}{\mathrm{d}t} = \frac{\mathrm{d}}{\mathrm{d}t}\left(\rho_v(R_*)\right) + N_d \frac{J_d}{ZV} - \frac{3D_0}{R_*} \frac{\rho_{v,*} - \rho_v(R_*)}{R_E - R_*} = \frac{\mathrm{d}}{\mathrm{d}t}\left(\rho_v(R_*)\right) - \frac{N_d}{\alpha_d ZV} \frac{\mathrm{d}m_d}{\mathrm{d}t} - \frac{3D_0}{R_*} \frac{\rho_{v,*} - \rho_v(R_*)}{R_E - R_*} \tag{13}$$

for the rate of change of coupling water vapor density.

To define the volume V in equation (10), we first give an alternate interpretation of the rate $\frac{J_d}{ZV}$ with the help of the artificial spherical shell from figure 3. Let

$$V_S := \frac{4}{3}\pi\left((R_* + r_E)^3 - (R_* - r_E)^3\right) \tag{14}$$

denote the volume of the artificial spherical shell. Using equation (9), the rate may be rewritten as

$$\frac{J_d}{ZV} = \frac{J_d}{V_S} \frac{\frac{4}{3}\pi r_E^3}{V}. \tag{15}$$

The first factor represents the rate if all exchanged water vapor would modify the vapor density inside the spherical shell, where we assume water vapor and temperature as uniform. The second factor amounts to a scaling of the first factor. Since V is the volume into which water vapor diffuses in unit time, we define it as a scaled influence sphere around the droplet as

$$V := \frac{4}{3}\pi(nr_E)^3 = \frac{4}{3}\pi n^3 r_E^3 \tag{16}$$

with the scaled influence radius nr_E, leading to the rate $\frac{J_d}{ZV} = \frac{J_d}{V_S}\frac{1}{n^3}$. With this definition, only a fraction $\frac{1}{n^3}$ of the released water vapor from the droplet will affect the coupling value inside the artificial spherical shell. The choice of the parameter n will be discussed in subsection 2.2.4 below. Although we tried to give some interpretation of the product $\frac{J_d}{V_S}\frac{1}{n^3}$ and particularly the factor $\frac{1}{n^3}$, this scaling factor may also be interpreted as a free parameter of our model without a specific physical meaning.

5  For the radii of influence R_E, r_E we define

$$R_E := R_i + l_i, \tag{17a}$$

$$r_E := r_d + l_d \tag{17b}$$

for some positive constants l_i, l_d. Likewise, we define the coupling radius by

$$R_* := R_i + l_0 \tag{18}$$

10 with $0 < l_0 < l_i$. With these definitions we can state the complete ODE system as

$$\frac{dm_d}{dt} = 4\pi\alpha_d D_0 r_d r_E \frac{\rho_{v,*} - \rho_{v,d}}{r_E - r_d}, \tag{19a}$$

$$\frac{dT_d}{dt} = \frac{4\pi r_d r_E}{m_d c_{p,l}(T_d)(r_E - r_d)}\Big(\alpha_d D_0 L_{lv}(T_d)(\rho_{v,*} - \rho_{v,d}) + K_0(T_* - T_d)\Big), \tag{19b}$$

$$\frac{dM_i}{dt} = 4\pi\alpha_i D_0 R_i R_* \frac{\rho_{v,*} - \rho_{v,i}}{R_* - R_i}, \tag{19c}$$

$$\frac{dT_i}{dt} = \frac{4\pi R_i R_*}{M_i c_{p,i}(T_i)(R_* - R_i)}\Big(\alpha_i D_0 L_{iv}(T_i)(\rho_{v,*} - \rho_{v,i}) + K_0(T_* - T_i)\Big), \tag{19d}$$

15 $$\frac{d\rho_{v,*}}{dt} = \frac{d}{dt}\Big(\rho_v(R_*)\Big) + N_d\frac{J_d}{ZV} - \frac{3D_0}{R_*}\frac{\rho_{v,*} - \rho_v(R_*)}{R_E - R_*}, \tag{19e}$$

$$\frac{dT_*}{dt} = \frac{d}{dt}\Big(T(R_*)\Big). \tag{19f}$$

Substituting R_* from (18) into the field representations in equation (1) yields an expression of $\rho_v(R_*)$ and $T(R_*)$, allowing to compute the required derivatives. Keeping equations (17) and (18) in mind, we arrive at

$$\frac{d}{dt}\Big(\rho_v(R_*)\Big) = \frac{R_E}{R_E - R_i}\Big(1 - \frac{R_i}{R_*}\Big)\frac{d\rho_{v,\infty}}{dt} + \frac{R_i}{R_E - R_i}\Big(\frac{R_E}{R_*} - 1\Big)\frac{d\rho_{v,i}}{dt} + \frac{\rho_{v,i} - \rho_{v,\infty}}{R_E - R_i}\Big(\frac{R_E + R_i}{R_*} - \frac{R_i R_E}{R_*^2} - 1\Big)\frac{dR_i}{dt} \tag{20}$$

20 and

$$\frac{d}{dt}\Big(T(R_*)\Big) = \frac{R_E}{R_E - R_i}\Big(1 - \frac{R_i}{R_*}\Big)\frac{dT_\infty}{dt} + \frac{R_i}{R_E - R_i}\Big(\frac{R_E}{R_*} - 1\Big)\frac{dT_i}{dt} + \frac{T_i - T_\infty}{R_E - R_i}\Big(\frac{R_E + R_i}{R_*} - \frac{R_i R_E}{R_*^2} - 1\Big)\frac{dR_i}{dt}. \tag{21}$$

The derivative of the ice crystal radius may be calculated using the equation for the mass of a spherical ice crystal $M_i = \frac{4}{3}\pi\rho_i(T_i)R_i^3$ with ice density ρ_i, yielding

$$\frac{dR_i}{dt} = \frac{1}{4\pi\rho_i(T_i)R_i^2}\frac{dM_i}{dt} = \frac{\alpha_i D_0}{\rho_i(T_i)}\frac{R_*}{R_i}\frac{\rho_{v,*} - \rho_{v,i}}{R_* - R_i} \tag{22}$$

where we neglected the derivative of the ice density ρ_i.

Neglecting chemical composition and curvature effects of the ice crystal, we approximate the saturation vapor density $\rho_{v,i}$ at the surface by

$$\rho_{v,i} \approx \frac{p_{i,\text{sat}}(T_i)}{R_v T_i}, \tag{23}$$

where $p_{i,\text{sat}}$ denotes the saturation vapor pressure over a plane ice surface. Using the Clausius-Clapeyron equation (Lamb and Verlinde, 2011, equations (4.35) and (4.36)), we obtain the temporal derivative

$$\frac{\mathrm{d}\rho_{v,i}}{\mathrm{d}t} \approx \frac{\mathrm{d}}{\mathrm{d}t}\left(\frac{p_{i,\text{sat}}(T_i)}{R_v T_i}\right)\frac{\mathrm{d}T_i}{\mathrm{d}t} = \frac{p_{i,\text{sat}}(T_i)}{R_v T_i^2}\left(\frac{L_{iv}(T_i)}{R_v T_i} - 1\right)\frac{\mathrm{d}T_i}{\mathrm{d}t}. \tag{24}$$

2.2 Choice of Parameters

In this subsection we discuss a possible choice of the parameters l_i, l_d, l_0, N_d and n from equations (17), (18), (19e), (16), respectively. We estimate possible values for these parameters using typical environmental conditions in a mixed-phase cloud with ambient temperature $T_\infty = -15\,°\text{C}$, ambient pressure $p_\infty = 650\,\text{hPa}$, ambient saturation ratio $S_\infty = 1.01$, ice crystal radius $R_i = 100\,\mu\text{m}$ and droplet radius $r_d = 10\,\mu\text{m}$.

2.2.1 Parameter for Droplet Distance

Parameter l_0 in equation (18) defines the distance from the droplet center to the ice crystal surface. To estimate this parameter, we assume a perfectly regular distribution of droplets at the vertices of a cubic lattice with $\mathcal{N} = 1000\,\text{cm}^{-3} = 10^9\,\text{m}^{-3}$ droplets inside the cloud volume. This droplet number is higher than typical observed values, but since our focus is on local droplet accumulations around ice crystals, we use this higher value. Let

$$l_K := \frac{1}{\sqrt[3]{\mathcal{N}} - 1\,\text{m}^{-1}} \tag{25}$$

denote the edge length of a cuboid in the lattice. If the ice crystal is located in the center of such a cuboid, the distance from the midpoint of the ice crystal to the midpoint of the nearest droplet is given by $\frac{\sqrt{3}}{2}l_K$, yielding an estimate for $R_* = R_i + l_0$. Substituting values, we arrive at $l_0 \approx 7.67 \cdot 10^{-4}\,\text{m} = 767\,\mu\text{m}$ being approximately 7.5 times ice radii, so $l_0 = 7.5 R_i$.

2.2.2 Parameter for Radii of the Influence Spheres

To estimate the distance parameter l_i, determining the radius of the influence sphere of the ice crystal, we use the representation

$$\rho_v(R) = \rho_{v,\infty} - \frac{R_i(\rho_{v,\infty} - \rho_{v,i})}{R} \tag{26}$$

of the water vapor field obtained from Maxwellian growth theory. Let $\xi > 0$ denote a chosen maximal relative deviation of $\rho_v(R)$ from the environmental value $\rho_{v,\infty}$, we seek the radius R_E such that

$$\frac{|\rho_v(R) - \rho_{v,\infty}|}{\rho_{v,\infty}} \leq \xi \tag{27}$$

is satisfied for $R \geq R_E$. Substituting (26) into (27) yields the condition

$$\frac{R_i}{\xi \rho_{v,\infty}} |\rho_{v,\infty} - \rho_{v,i}| \leq R_E. \tag{28}$$

Neglecting effects of chemical substances and curvature, we estimate the surface water vapor density as $\rho_{v,i} = \frac{p_{i,\text{sat}}(T_\infty)}{R_v T_\infty}$.

Using a maximal relative deviation $\xi = 10^{-3}$, we arrive at $l_i \approx 0.0144\,\text{m}$ being approximately 144 ice radii, so $l_i = 144 R_i$. Using the same approach for the droplets, we obtain $l_d \approx 8.9 \cdot 10^{-5}\,\text{m}$ being approximately 9 droplet radii, so $l_d = 9 r_d$. We chose $\xi = 10^{-3}$ as the maximal relative deviation, because the relative deviations

$$\frac{|\rho_{v,\infty} - \rho_{v,i}|}{\rho_{v,\infty}} \quad \text{and} \quad \frac{|\rho_{v,\infty} - \rho_{v,d}|}{\rho_{v,\infty}} \tag{29}$$

are already of the order $1.4 \cdot 10^{-1}$ and 10^{-2}, respectively, for the conditions stated at the beginning of the subsection. For the case of a droplet, Reiss and La Mer (1950) and Reiss (1951) suggest a value of ten times droplet diameter for the radius of influence. With our choice of the relative deviation, we obtain the same order of magnitude.

2.2.3 Number Parameter

In order to estimate a typical droplet number N_d within the influence sphere around the ice crystal, we employ the typical droplet number concentration $\mathcal{N} = 70\,\text{cm}^{-3}$ in mixed-phase clouds (Korolev et al., 2003; Zhao and Lei, 2014). Using $l_i = 144 R_i$, we obtain a droplet number

$$N_d = \mathcal{N} \frac{4}{3} \pi (R_i + l_i)^3 = \mathcal{N} \frac{4}{3} \pi (145 \cdot R_i)^3 \approx 894. \tag{30}$$

Not all of these droplets are precisely at coupling distance R_* from the midpoint of the ice crystal and the influence of droplets decreases with increasing distance from ice crystal center. Qualitatively, only the droplets closest to the ice crystal influence its growth behavior significantly, see Baumgartner and Spichtinger (2017b, their figure 6). We employ the conservative assumption that all droplets with distances smaller than $\frac{R_*}{3}$ have larger influence on the ice crystal and consequently define the droplet number N_d as

$$N_d = \mathcal{N} \frac{4}{3} \pi \left(\frac{R_i + l_0}{3} \right)^3 = \mathcal{N} \frac{4}{3} \pi \left(\frac{145}{3} R_i \right)^3 \approx 32, \tag{31}$$

motivating the choice $N_d = 40$. We remark that this droplet number is highly variable in real clouds due to turbulent effects or sedimentation of the ice crystal. If one knew an expression, describing the change of droplet number inside the influence sphere, one could also use a variable number instead of a constant.

2.2.4 Distribution Parameter

Parameter n in equation (16) is a critical parameter of the whole model, since it determines directly the strength of the interaction between the ice crystal and the droplet. According to the interpretation given above, it describes which fraction of released water vapor from an evaporating droplet is incorporated into the artificial spherical shell around the ice crystal and
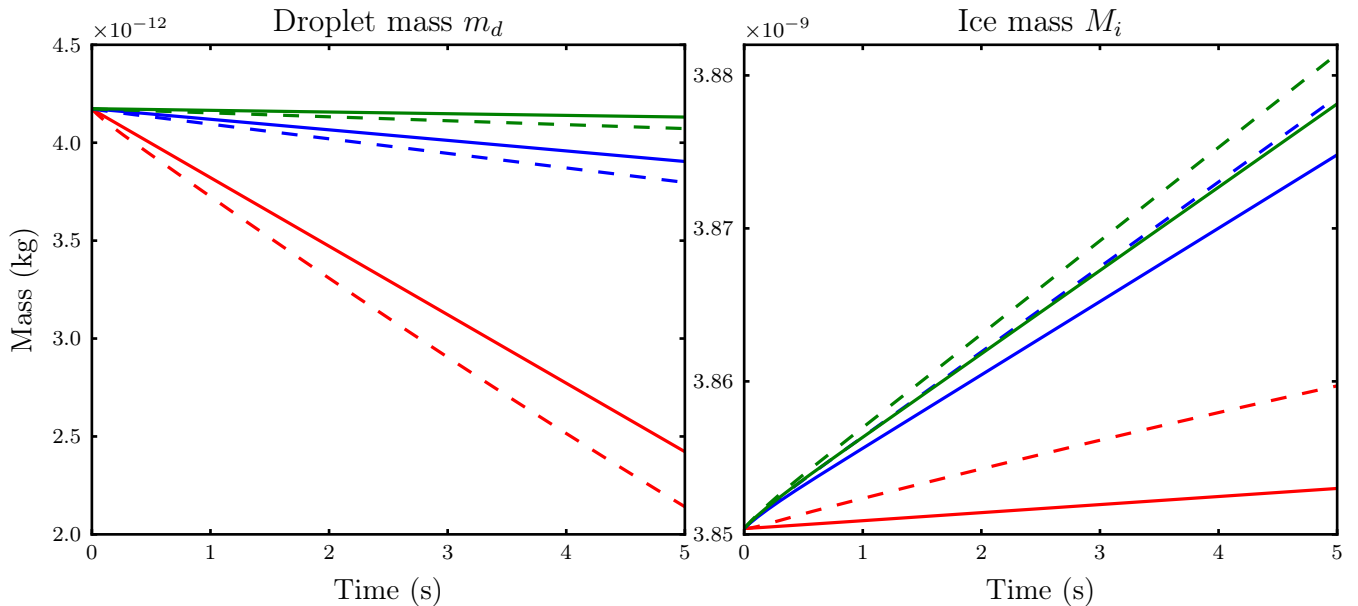
Figure 4. Comparison of the temporal evolution of hydrometeor masses obtained with the new model from equation (19) with parameter value $n = 1.8$ (dashed) and the reference model (solid) for the case of $N_d = 14$ droplets per influence sphere. Ambient saturation ratios are $S_\infty = 0.86$ (red), $S_\infty = 0.99$ (blue) and $S_\infty = 1.01$ (green).

consequently influences the growth of the ice crystal, see equation (15). If $n = 1$, all released water vapor is incorporated in the artificial spherical shell. If $n > 1$, only a fraction of $\frac{1}{n^3}$ is incorporated, and the remaining water vapor is released to the atmosphere. In this study, we use a value $n = 1.8$, obtained with the help of direct numerical simulations using the reference model described in Baumgartner and Spichtinger (2017b), since the authors are not aware of any direct measurements.

5   We compare the temporal evolution of the ice crystal and droplet mass obtained from the reference model with results of the model presented in section 2.1 using the two droplet numbers $N_d = 14$ and $N_d = 38$. The choice of these droplet numbers is due to the existence of Lebedev quadrature formulas, because those quadrature points allow a nearly uniform distribution along a sphere (Lebedev, 1976). For calculations with the reference model, we distributed the droplets along a sphere with radius $7.5 R_i$ around the ice crystal. We conducted several simulations using the new model with different values for the parameter

10   n. Figures 4 and 5 show the accordance of droplet and ice crystal mass evolution for our final parameter value $n = 1.8$ at ambient saturation ratios $S_\infty = 0.86$, $S_\infty = 0.99$ and $S_\infty = 1.01$ for the two droplet numbers $N_d = 14$ and $N_d = 38$. The solid and dashed curves agree well although the droplet masses are slightly underestimated and the ice crystal mass is slightly overestimated.

Although not shown, numerical experiments with other values of the parameter n show, that we can achieve better agreement

15   of either the ice mass or droplet curves, but not for both simultaneously. Moreover, our choice $n = 1.8$ also shows satisfactory results in other mass and humidity regimes.
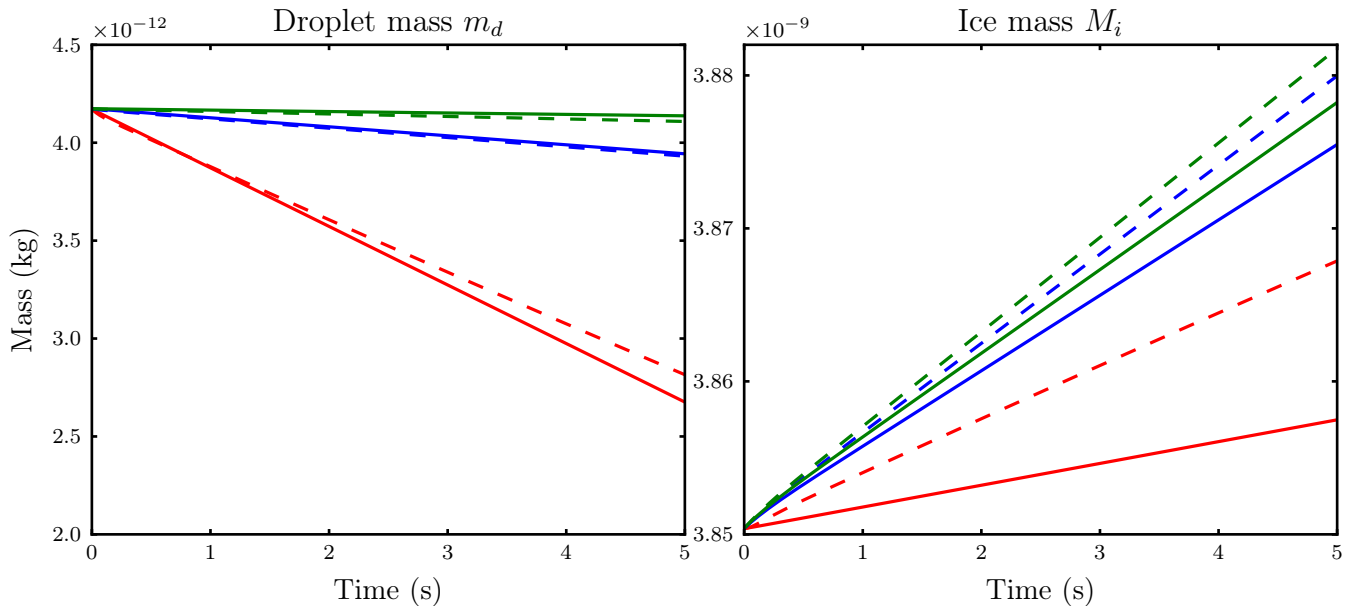
Figure 5. As in figure 4, but for the case of $N_d = 38$ droplets per influence sphere.

2.3 Simplifications

The model in equation (19) consists of many equations, especially it keeps track of the temperature of the individual hydrometeors. In Maxwellian growth theory, the equation for the temperature of a hydrometeor is eliminated. We can simplify the model equations (19) in a similar way. Proceeding as in the derivation of the Maxwellian growth equations, we can eliminate the temperature equations of the hydrometeors. The modified equations for the hydrometeor masses are then given by

$$\frac{\mathrm{d}m_d}{\mathrm{d}t} = \frac{4\pi}{\left(\frac{L_{lv}(T_\infty)}{R_v T_\infty} - 1\right)\frac{L_{lv}(T_\infty)}{K_0 T_\infty} + \frac{R_v T_\infty}{\alpha_d D_0 p_{l,\mathrm{sat}}(T_\infty)}}\frac{r_d r_E}{r_E - r_d}(S_* - 1) =: G_l \frac{r_d r_E}{r_E - r_d}(S_* - 1) \tag{32}$$

for droplet mass and

$$\frac{\mathrm{d}M_i}{\mathrm{d}t} = \frac{4\pi}{\left(\frac{L_{iv}(T_\infty)}{R_v T_\infty} - 1\right)\frac{L_{iv}(T_\infty)}{K_0 T_\infty} + \frac{R_v T_\infty}{\alpha_i D_0 p_{i,\mathrm{sat}}(T_\infty)}}\frac{R_i R_*}{R_* - R_i}(S_{*,i} - 1) =: G_i \frac{R_i R_*}{R_* - R_i}(S_{*,i} - 1) \tag{33}$$

for ice crystal mass with the saturation ratios $S_* = \frac{\rho_{v,*} R_v T_\infty}{p_{l,\mathrm{sat}}(T_\infty)}$ and $S_{*,i} = \frac{\rho_{v,*} R_v T_\infty}{p_{i,\mathrm{sat}}(T_\infty)}$, respectively, where $p_{l,\mathrm{sat}}$ denotes the saturation vapor pressure over a plane surface of liquid water. In addition, we neglect the temperature equation (19f) for the coupling temperature T_* in the governing system (19). Since T_* also appears in the calculation of the unperturbed value $\rho_v(R_*)$ through the equilibrium vapor density at the ice crystal surface, we have to modify its calculation from equation (1). We simplify the vapor density field from equation (1) by considering the case $R_E \to \infty$, representing the observation $R_i \ll R_E$. The vapor density at the ice crystal surface is approximated as in (23), yielding

$$\rho_v(R_*) \approx \rho_{v,\infty} + (\rho_{v,i} - \rho_{v,\infty})\frac{R_i}{R_*} \approx \rho_{v,\infty} + \left(\frac{p_{i,\mathrm{sat}}(T_\infty)}{R_v T_\infty} - \rho_{v,\infty}\right)\frac{R_i}{R_*}. \tag{34}$$

Using the Clausius-Clapeyron equation and (22), we compute the required time derivative of (34) as

$$
\begin{aligned}
\frac{\mathrm{d}}{\mathrm{d}t}\left(\rho_v(R_*)\right) &\approx \left(1-\frac{R_i}{R_*}\right)\frac{\mathrm{d}\rho_{v,\infty}}{\mathrm{d}t} + \frac{R_i}{R_*}\frac{\mathrm{d}}{\mathrm{d}t}\left(\frac{p_{i,\mathrm{sat}}(T_\infty)}{R_v T_\infty}\right) + \left(\frac{p_{i,\mathrm{sat}}(T_\infty)}{R_v T_\infty} - \rho_{v,\infty}\right)\frac{R_*-R_i}{R_*^2}\frac{\mathrm{d}R_i}{\mathrm{d}t} \\
&= \left(1-\frac{R_i}{R_*}\right)\frac{\mathrm{d}\rho_{v,\infty}}{\mathrm{d}t} + \frac{R_i}{R_*}\frac{p_{i,\mathrm{sat}}(T_\infty)}{R_v T_\infty^2}\left(\frac{L_{iv}(T_\infty)}{R_v T_\infty}-1\right)\frac{\mathrm{d}T_\infty}{\mathrm{d}t} + \left(\frac{p_{i,\mathrm{sat}}(T_\infty)}{R_v T_\infty}-\rho_{v,\infty}\right)\frac{R_*-R_i}{4\pi\rho_i(T_\infty)R_i^2 R_*^2}\frac{\mathrm{d}M_i}{\mathrm{d}t}.
\end{aligned}
\tag{35}
$$

Accepting those further approximations, we arrive at the simplified system

$$
\frac{\mathrm{d}m_d}{\mathrm{d}t} = G_l \frac{r_d r_E}{r_E - r_d}\left(S_* - 1\right),
\tag{36a}
$$

$$
\frac{\mathrm{d}M_i}{\mathrm{d}t} = G_i \frac{R_i R_*}{R_* - R_i}\left(S_{*,i} - 1\right),
\tag{36b}
$$

$$
\frac{\mathrm{d}\rho_{v,*}}{\mathrm{d}t} = \frac{\mathrm{d}}{\mathrm{d}t}\left(\rho_v(R_*)\right) - \frac{N_d}{\alpha_d Z V}\frac{\mathrm{d}m_d}{\mathrm{d}t} - \frac{3D_0}{R_*}\frac{\rho_{v,*}-\rho_v(R_*)}{R_E-R_*},
\tag{36c}
$$

where only the three prognostic variables m_d, M_i and $\rho_{v,*}$ are left. For a bulk model parameterisation, we would add just one additional equation.

2.4 Discussion of the Model Ansatz

Already Srivastava (1989) criticized the use of Maxwellian growth theory for the description of droplet growth by diffusion. He advocated the use of local quantities instead of the environmental conditions, since water vapor density is spatially variable and the droplet growth heavily depends on its precise value. By using local variables, one can take those variations into account and compute growth rates of hydrometeors more accurately. He connected the local value for vapor density to the environmental value through a relaxation of local conditions to the environmental conditions, similarly as we did in equation (12) for I_3. Srivastava proposed to consider local volumes around every hydrometeor and to compute its individual growth rate by using the local vapor density. We adopted this approach in our model by introducing the "spheres of influence". Similar ideas were employed in Marshall and Langleben (1954), where the authors also consider a local volume around an ice crystal. In contrast to our formulation, they assume a continuous droplet distribution inside the local volume. Their method avoids additional growth equations for the nearby droplets. Our approach combines ideas of both former studies, where we focused on a model formulation which only incorporates values that are typically known in a numerical cloud model.

In subsection 2.2, we estimated possible values for the parameters of our model. To our best knowledge, there are no direct measurements of the local interactions of a single ice crystal with surrounding droplets available, so we cannot compare our parameter choice with real measurements. Instead we can consider two separate extreme cases, since equation (19e) for the coupling water vapor density has the generic representation

$$
\frac{\mathrm{d}\rho_{v,*}}{\mathrm{d}t} = \frac{\mathrm{d}}{\mathrm{d}t}\left(\rho_v(R_*)\right) - \frac{N_d}{Z V}\frac{\mathrm{d}m_d}{\mathrm{d}t} - C\left(\rho_{v,*}-\rho_v(R_*)\right)
\tag{37}
$$

for a constant $C > 0$. In our model derivation, we set $C := \frac{3D_0}{R_*(R_E-R_*)}$. The two extreme cases are constructed by choosing $C = 0$ or $C \to \infty$. In the first case $C = 0$, relaxation of the coupling value $\rho_{v,*}$ to the equilibrium value $\rho_v(R_*)$ is neglected

and therefore $\rho_{v,*}$ is solely changed by the growth or evaporation of the hydrometeors. The second case $C \to \infty$ corresponds to an instantaneous relaxation to equilibrium. This is basically the same behavior as in the classical treatment using Maxwellian growth theory. We emphasize that both extreme cases are rather nonphysical, but they may serve to assess the possible strength of the local interactions. However, we believe that ansatz (37) is able to capture the essential behavior, possibly after considering

5 $\frac{1}{ZV}$ as a single coefficient which is to be determined with the help of measurements.

We believe that the most promising measurement technology to constrain the parameters in our model is holography, because it is able to measure the spatial distribution and the size of hydrometeors within an air volume (Fugal and Shaw, 2009; Schlenczek et al., 2017; Beals et al., 2015). Moreover, if it will be possible to track an individual air volume with holographic imaging, one could possibly infer values for our model constants from the size evolutions of the hydrometeors.

10 In subsection 2.2.3 we discussed the choice of the number N_d of droplets within the influence sphere of the ice crystals. Imaging the influence sphere around the ice crystal as an object moving with the ice crystal, clearly the number of droplets inside this region should change as the ice crystal moves through a cloudy volume. If we could establish an equation for $\frac{dN_d}{dt}$, the number N_d of droplets within the influence sphere could be made dynamic. Such an equation should account not only for the movement of the ice crystal through the cloudy volume but also for the influence of turbulence on the local droplet number.

15 Note that the concept of an influence sphere around the ice crystal remains meaningful for moving ice crystals. The presence of the ice crystal distorts the local water vapor and temperature field and thus defines its influence sphere. As is well known from Maxwellian growth theory, the fields around the ice crystal attain very rapidly their steady-state (Lamb and Verlinde, 2011, Chapter 8.2.2), so we can define the influence sphere with the help of the steady-state field.

3   Incorporation into a Parcel Model

20 In this section, we incorporate the new model of section 2 into a parcel model. Let p_∞ and T_∞ denote pressure and temperature of the air parcel. We divide the total water mass contained in the air parcel into the mass of water vapor M_v, the mass of liquid water M_l and the mass of ice M_{ice}. In addition, the air parcel contains a mass M_a of dry air. Since the air parcel is assumed as thermodynamically closed, the mass M_a of dry air and the total water mass $M_v + M_l + M_{\text{ice}}$ are constant. Instead of the masses, we consider the mixing-ratios $q_x := \frac{M_x}{M_a}$ for $x \in \{v, l, \text{ice}\}$.

25 ### 3.1   Description of the Parcel Model

Variations in pressure p_∞ are governed by the equation

$$\frac{dp_\infty}{dt} = \frac{dp_\infty}{dz}\frac{dz}{dt} = -g\frac{p_\infty}{\overline{R}T_\infty}w, \tag{38}$$

obtained by applying the equation for hydrostatic equilibrium. Coordinate z denotes the height, g the acceleration of gravity, w the vertical velocity and $\overline{R}$ the gas constant for moist air, given by

30 $$\overline{R} := R_a\left(1 + \frac{1-\varepsilon}{\varepsilon}\frac{q_v}{1+q_v}\right) \tag{39}$$

where $\varepsilon := \frac{R_a}{R_v}$ and R_a, R_v denote the gas constants for dry air and water vapor, respectively. A change in the air parcel temperature T_∞ has two contributions. The first contribution comes from the adiabatic vertical motion of the air parcel and is given by (for example Wang, 2013, chapter 12)

$$\left.\frac{\mathrm{d}T_\infty}{\mathrm{d}t}\right|_{\text{adiabatic}} = -\frac{g}{\overline{c_p}}w \tag{40}$$

5   where the specific heat capacity of moist air is given by (Rogers and Yau, 1989, chapter 2)

$$\overline{c_p} := c_{p,a}\left(1 + \left(\frac{c_{p,v}}{c_{p,a}} - 1\right)\frac{q_v}{1 + q_v}\right) \tag{41}$$

and $c_{p,a}, c_{p,v}$ denote the specific heat capacity of dry and moist air, respectively. If condensation of water vapor takes place, we have to include latent heat effects. Let ω_k be a hydrometeor, then its temperature T_k changes as

$$c_{p,k}m_k\frac{\mathrm{d}T_k}{\mathrm{d}t} = L\frac{\mathrm{d}m_k}{\mathrm{d}t} + \int_{\partial\omega_k} K\nabla T \cdot N\,\mathrm{d}\sigma, \tag{42}$$

10   where m_k is the mass of hydrometeor ω_k, L the latent heat of a phase change, K the thermal conductivity of air and N the outer normal to the surface of the hydrometeor ω_k. The surface integral in (42) accounts for heat conduction from the hydrometeor to the air parcel. The amount of heat $-\mathrm{d}Q_{\text{conduction}}$, delivered from the single hydrometeor ω_k to the air parcel, is given by the rate

$$-\frac{\mathrm{d}Q_{\text{conduction}}}{\mathrm{d}t} = \int_{\partial\omega_k} K\nabla T \cdot N\,\mathrm{d}\sigma. \tag{43}$$

15   This amount of heat changes the temperature T_∞ of the air parcel according to $\overline{c_p}\left(M_v + M_a\right)\mathrm{d}T_\infty = -\mathrm{d}Q_{\text{conduction}}$. Inserting (43) and summing over all hydrometeors yields the rate

$$\left.\frac{\mathrm{d}T_\infty}{\mathrm{d}t}\right|_{\text{latent}} = -\frac{1}{\overline{c_p}\left(M_v + M_a\right)}\sum_k \int_{\partial\omega_k} K\nabla T \cdot N\,\mathrm{d}\sigma \tag{44}$$

of latent heating. Combining both contributions (40) and (44) yields the final rate of the temperature change

$$\frac{\mathrm{d}T_\infty}{\mathrm{d}t} = \left.\frac{\mathrm{d}T_\infty}{\mathrm{d}t}\right|_{\text{adiabatic}} + \left.\frac{\mathrm{d}T_\infty}{\mathrm{d}t}\right|_{\text{latent}} = -\frac{g}{\overline{c_p}}w - \frac{1}{\overline{c_p}(M_v + M_a)}\sum_k \int_{\partial\omega_k} K\nabla T \cdot N\,\mathrm{d}\sigma \tag{45}$$

20   where the sum expands over all hydrometeors. In the literature, one finds a slightly different equation, where the surface integral is replaced by $-L\frac{\mathrm{d}m_k}{\mathrm{d}t}$ (for example Pruppacher and Klett, 1997, equation 12.15). Assuming all hydrometeors to have reached their equilibrium temperature, as is done in classical Maxwellian growth theory, the time derivative on the left hand side of (42) vanishes and equation (45) reduces to the equation from literature.

    We further divide the liquid water mass M_l contained in the air parcel into the mass M_l^i of all droplets located in an influence sphere of some ice crystal and the mass M_l^o of all droplets outside of every ice crystal influence sphere. From now on, we assume a monodisperse mass distributions for the ice crystals with number concentration $\mathcal{N}_{\text{ice}}$, for the droplets inside

the ice crystal influence spheres with number concentration $\mathcal{N}_{\text{ice}} N_d$ (number of ice influence spheres containing N_d droplets each) and and for the droplets outside of every ice crystal influence sphere with number concentration $\mathcal{N}_d^o$. Therefore, the total droplet number concentration in the air parcel is $\mathcal{N}_{\text{ice}} N_d + \mathcal{N}_d^o$ (number per kilogram of dry air). Because of the assumption of monodisperse size distributions, each ice particle has mass M_i, each droplet inside an influence sphere has mass m_d^i and each

5 droplet outside of every influence sphere has mass m_d^o. Defining the liquid water mixing-ratios $q_l^i := \frac{M_l^i}{M_a}$ and $q_l^o := \frac{M_l^o}{M_a}$, we obtain the relations

$$q_{\text{ice}} = \mathcal{N}_{\text{ice}} M_i, \quad \text{and} \quad q_l = q_l^o + q_l^i = \mathcal{N}_d^o m_d^o + N_d \mathcal{N}_{\text{ice}} m_d^i \tag{46}$$

where N_d is the number of droplets inside the influence sphere of an ice crystal. As for the liquid water mass, we divide the corresponding droplet temperatures in T_d^i, T_d^o and the droplet radii in r_d^i, r_d^o.

10 Using this notation and the assumption of spherical droplets, we can evaluate the surface integrals in (45) to obtain

$$
\begin{aligned}
\frac{\mathrm{d}T_\infty}{\mathrm{d}t} &= -\frac{g}{\overline{c_p}} w - \frac{1}{\overline{c_p}(M_v + M_a)} \Big(\mathcal{N}_d^o M_a 4\pi r_d^o K_0 (T_\infty - T_d^o) \\
&\quad + N_d \mathcal{N}_{\text{ice}} M_a 4\pi r_d^i K_0 (T_\infty - T_d^i) + \mathcal{N}_{\text{ice}} M_a 4\pi R_i K_0 (T_\infty - T_i) \Big) \\
&= -\frac{g}{\overline{c_p}} w - \frac{4\pi K_0 M_a}{\overline{c_p}(M_v + M_a)} \Big(\mathcal{N}_d^o r_d^o (T_\infty - T_d^o) \\
&\quad + N_d \mathcal{N}_{\text{ice}} r_d^i (T_\infty - T_d^i) + \mathcal{N}_{\text{ice}} R_i (T_\infty - T_i) \Big) \\
&= -\frac{g}{\overline{c_p}} w - \frac{4\pi K_0}{\overline{c_p}(1 + q_v)} \Big(\mathcal{N}_d^o r_d^o (T_\infty - T_d^o) \\
&\quad + N_d \mathcal{N}_{\text{ice}} r_d^i (T_\infty - T_d^i) + \mathcal{N}_{\text{ice}} R_i (T_\infty - T_i) \Big),
\end{aligned}
\tag{47}
$$

where R_i denotes the radius of an ice crystal. The mixing-ratio for water vapor is determined by the conservation of mass and reads

$$\frac{\mathrm{d}q_v}{\mathrm{d}t} = -\frac{\mathrm{d}q_l^o}{\mathrm{d}t} - \frac{\mathrm{d}q_l^i}{\mathrm{d}t} - \frac{\mathrm{d}q_{\text{ice}}}{\mathrm{d}t} = -\mathcal{N}_d^o \frac{\mathrm{d}m_d^o}{\mathrm{d}t} - \mathcal{N}_{\text{ice}} \left(N_d \frac{\mathrm{d}m_d^i}{\mathrm{d}t} + \frac{\mathrm{d}M_i}{\mathrm{d}t} \right). \tag{48}$$

15 The equations for the other mixing-ratios are given by

$$\frac{\mathrm{d}q_{\text{ice}}}{\mathrm{d}t} = \mathcal{N}_{\text{ice}} \frac{\mathrm{d}M_i}{\mathrm{d}t}, \tag{49a}$$

$$\frac{\mathrm{d}q_l^o}{\mathrm{d}t} = \mathcal{N}_d^o \frac{\mathrm{d}m_d^o}{\mathrm{d}t}, \tag{49b}$$

$$\frac{\mathrm{d}q_l^i}{\mathrm{d}t} = N_d \mathcal{N}_{\text{ice}} \frac{\mathrm{d}m_d^i}{\mathrm{d}t}. \tag{49c}$$

3.2 Results

20 Using the parcel model we carry out several simulations, where we vary the coupling distance $R_* = R_i + l_0$ through parameter l_0, the number of droplets inside the influence sphere of the ice crystals N_d, the ambient saturation ratio S_∞ and the vertical velocity w of the air parcel, see table 1. The choice of the saturation ratios is motivated by the three regimes in figure 1.

Table 1. Different parameter values used for the air parcel simulations. The initial ice crystal radius is $R_i = 100\,\mu\mathrm{m}$ for every simulation.

l_0	$5R_i$	$15R_i$	$30R_i$	$50R_i$	$100R_i$	Length parameter for ice–droplet distance
N_d	40	100	200	500		Number of droplets per ice crystal influence sphere
S_∞	0.847	0.932	1.01			Ambient saturation ratio with respect to liquid water
$S_{\infty,i}$	0.98	1.079	1.169			Ambient saturation ratio with respect to ice
w	$0\,\mathrm{ms}^{-1}$	$-1\,\mathrm{ms}^{-1}$	$1\,\mathrm{ms}^{-1}$			Vertical velocity of the air parcel

The initial values for ambient temperature and pressure are $T_\infty = -15\,°\mathrm{C}$ and $p_\infty = 650\,\mathrm{hPa}$, respectively, resembling typical environmental conditions for a mixed-phase cloud. Reliable values for the droplet number N_d inside every influence sphere of the ice crystals are difficult to estimate, since this depends heavily on small-scale turbulence. Therefore, any of the estimated values in subsection 2.2.3 between $N_d = 30$ and $N_d = 800$ is possible, explaining the choices in table 1.

5 Previous studies indicate a large scattering of the microphysical parameters, especially in liquid water content (LWC) and ice water content (IWC) (for example Fleishauer et al., 2002; Hobbs et al., 2001; Pinto et al., 2001; Noh et al., 2013; Zhao and Lei, 2014; Lloyd et al., 2015; Verlinde et al., 2007). We use the typical values $\mathrm{LWC} = 0.045\,\mathrm{gm}^{-3}$ (Korolev et al., 2003) and $\mathrm{IWC} = 0.013\,\mathrm{gm}^{-3}$ (Fleishauer et al., 2002). A typical droplet radius is given by $10\,\mu\mathrm{m}$. Variability in size of the ice crystals is much larger, but on average, pristine ice crystals in mixed-phase clouds tend to be smaller than in ice clouds (Korolev et al., 10 2003) and we use again a value of $100\,\mu\mathrm{m}$ as initial radius.

In the subsequent sections, we present simulation results ordered by vertical velocity. All figures contain three curves: the red curve represents the solution of the new system (19), the cyan and blue curve represent the solutions of the same system, where the equation for the coupling water vapor density (19e) is replaced by (37) with $C = 0$ and $C \to \infty$, respectively. Consequently, those two curves correspond to the extreme cases without local relaxation to equilibrium (case $C = 0$) and 15 instantaneous relaxation to equilibrium (case $C \to \infty$). The spreading between the two curves show the spectrum of possible values for different choices of the parameter C.

3.2.1 Vertical Velocity $w = 0\,\mathrm{ms}^{-1}$

In Baumgartner and Spichtinger (2017b), the authors documented the largest effect of surrounding droplets on ice growth in an ice subsaturated environment, because the evaporating droplets can deliver enough water vapor towards the ice crystal to 20 produce a local supersaturation with respect to ice, allowing the crystal to grow instead of evaporate. With the new model, we also observe a similar behavior. Consider for example the case of $N_d = 40$ droplets per influence sphere of any ice crystal with the small droplet distance $l_0 = 5R_i = 5 \cdot 100\,\mu\mathrm{m}$ from the ice crystal and ambient saturation ratio $S_\infty = 0.847$, being subsaturated with respect to ice and water. The first row in figure 6 shows the temporal evolution of ice mixing-ratio q_i and liquid water mixing-ratio q_l. We observe an increasing ice mixing-ratio q_i, showing the aforementioned local interaction. As 25 long as not all droplets inside the influence spheres are evaporated, the red curve for ice mixing-ratio on the left of the upper
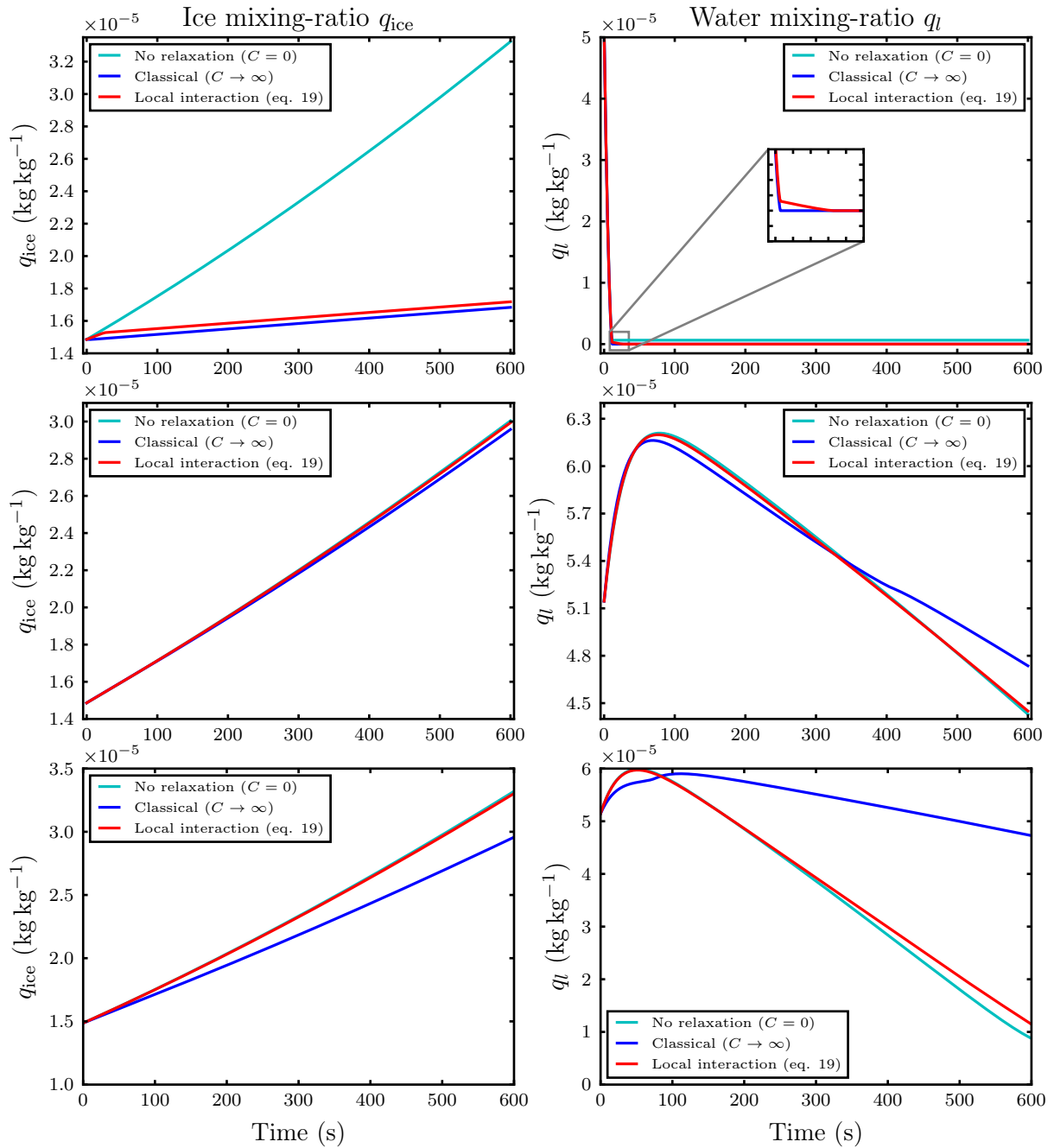
Figure 6. Temporal evolution of ice mixing-ratio (left) and liquid water mixing-ratio (right) for the parcel model simulations with $w = 0\,\mathrm{ms}^{-1}$. Parameters for the first row are $N_d = 40$ droplets in each influence sphere of the ice crystals at initial ambient saturation ratio $S_\infty = 0.847$ and droplet distance $l_0 = 5R_i$. The second and third row both have $N_d = 500$ droplets per influence sphere at $S_\infty = 1.01$, while the droplet distance is $l_0 = 30R_i$ for the second row and $l_0 = 5R_i$ for the third row. Note the different scaling of the axes.
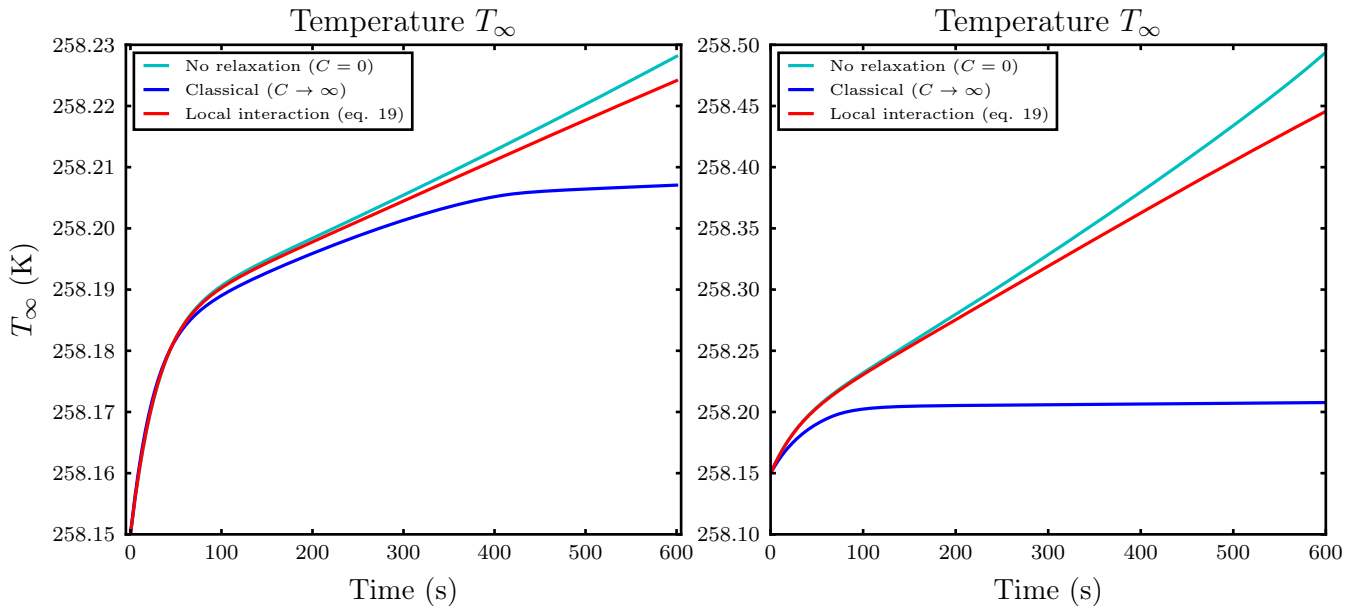
Figure 7. Temporal evolution of the air parcel temperature T_∞ with $w = 0\,\mathrm{ms}^{-1}$, $N_d = 500$ per influence sphere of the ice crystals at initial ambient saturation ratio $S_\infty = 1.01$ with droplet distance $l_0 = 30R_i$ (left) and $l_0 = 5R_i$ (right). Note the different scaling of the axes.

row in figure 6 coincides with the cyan curve, indicating the extreme case without local relaxation. This means the evaporating droplets inside the influence sphere of the ice crystal provide enough water vapor to mostly compensate diffusion of water vapor to the environment. The red curve in the left panel of the upper row in figure 6 shows the temporal evolution of liquid water mixing-ratio q_l. At the first kink of this curve (at about $t = 11\,\mathrm{s}$), all droplets outside of the influence spheres are evaporated

5   ($q_l^o = 0$) and at the second kink (at about $t = 26\,\mathrm{s}$) also the droplets inside the influence spheres are evaporated, indicating $q_l = q_l^o = q_l^i = 0$. Although the environment is subsaturated with respect to ice, the evaporating ice crystals alleviate the local subsaturation, allowing the droplets inside the influence spheres to exist slightly longer, see case (c) in the schematic figure 1. The kink in the red curve for ice-mixing ratio in the upper left panel in figure 6 at about $t = 26\,\mathrm{s}$ marks the time instant where all droplets are evaporated. From this time on, the local source for water vapor vanishes and the ice crystals grow slower. Note

10   that the evaporated droplets provided enough water vapor to the whole air parcel to cause an ice supersaturated environment, see figure B1 in the appendix, explaining why the ice crystals continue to grow although the air parcel was initially subsaturated with respect to ice.

     Changing the environmental conditions to water supersaturation with $S_\infty = 1.01$, local effects on the mixing-ratios are almost not visible. Only for small distances as $l_0 = 5R_i$ of the droplets in the influence spheres from the ice crystals or very

15   high droplet numbers N_d, an effect on the mixing-ratios is observed; for the case of a droplet–ice distance of $l_0 = 30R_i$ and droplet number $N_d = 500$, see the middle row in figure 6. The more interesting variable in this humidity regime is the temperature T_∞ of the air parcel, shown in the left panel of figure 7 for the aforementioned case. Compared to the classical

treatment, including the local effects yields a slightly warmer air parcel. The heating is caused by the release of latent heat of the growing hydrometeors. It persists after $100\,\mathrm{s}$ where the droplet mass starts to decrease and the evaporating droplets tend to cool the air parcel (right figure in the middle row of figure 6). Therefore, the observed heating is due to the growth of the ice crystals and should increase for increasing ice growth rate.

5   This motivates to consider the case of a small droplet–ice distance $l_0 = 5R_i$ and high droplet number $N_d = 500$ at ambient saturation ratio $S_\infty = 1.01$. The effect on the air parcel temperature T_∞ for this case is shown in the right panel of figure 7. The lower row in figure 6 an increase in ice mixing-ratio and a decrease in liquid water mixing-ratio already after a short time. This again confirms that the observed heating of the air parcel is caused by an increased growth rate of the ice crystals. The increase of the ice crystal growth rate is influenced by the number N_d of droplets within the influence sphere and the ambient

10   saturation ratio. If the air parcel is initially supersaturated with respect to water, the ice crystal induces a local subsaturation with respect to water and the droplets inside the influence sphere start to evaporate, see case (a) in the schematic in figure 1. Evaporation of nearby droplets enhances the local water vapor density and consequently also the ice growth rate. If the air parcel is initially subsaturated with respect to water, the droplets inside the influence sphere of an ice crystal see two sinks of water vapor, namely the ice crystal and the environment, see case (b) in the schematic figure 1. The released water vapor of

15   an evaporating droplet is therefore partially delivered to the ice crystal as well as the environment and the growth rate of the ice crystal is less amplified. Consequently, we expect a larger effect of the local interactions on the air parcel temperature with initially water supersaturated conditions.

3.2.2   Vertical Velocity $w = -1\,\mathrm{m\,s}^{-1}$

In a descending air parcel, saturation ratio decreases monotonically due to the adiabatic heating, causing an initially supersat-

20   urated air parcel to become subsaturated after a short time. According to the discussion in the previous subsection, we expect only negligible influence of the local effects on the temperature T_∞ of the air parcel. This was confirmed by our conducted simulations.

Contrary to the case of vanishing vertical velocity discussed in the previous subsection, local effects are clearly visible in the mixing-ratios for an initially supersaturated air parcel. In the following, we show two examples, the first with a small

25   droplet–ice distance and droplet number, the second with an increased droplet–ice distance and droplet number.

As the first example we choose a droplet–ice distance $l_0 = 5R_i$, droplet number $N_d = 200$ and initial ambient saturation ratio $S_\infty = 1.01$. The temporal evolution of the mixing-ratios is shown in the upper row in figure 8. From the ice mixing-ratio curve in the left panel in figure 8 it is evident, that ice crystals evaporate much slower in comparison with the classical case without local interactions (blue curve). Also the droplets inside the influence spheres of ice crystals can exist longer compared

30   to the classical case, see the right panel of the upper row in figure 8. The droplets inside the influence sphere evaporate slower because their released water vapor raises the local coupling value $\rho_{v,*}$ and consequently slows down further evaporation. This explains the first kink at about $t = 105\,\mathrm{s}$ of the red curve in the right upper panel in figure 8, where all outer droplets are evaporated. The second kink at about $t = 197\,\mathrm{s}$ marks the complete evaporation of all droplets. In this example, the droplets in the influence sphere exist up to $100\,\mathrm{s}$ longer than the droplets outside. As is indicated by the cyan curve, the time span may
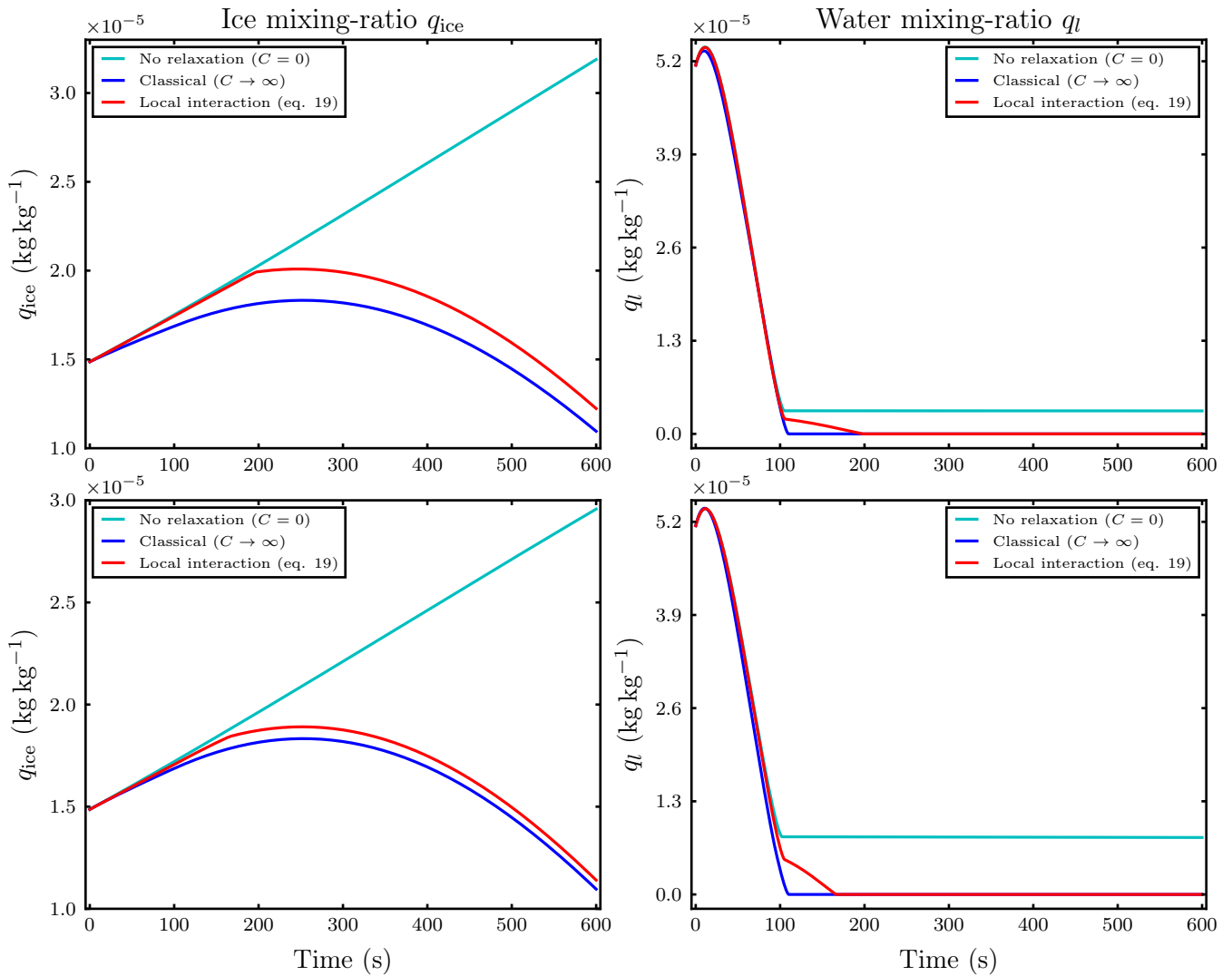
Figure 8. Temporal evolution of ice mixing-ratio (left) and liquid water mixing-ratio (right) for the parcel model simulations with $w = -1\,\mathrm{m\,s^{-1}}$ at initial ambient saturation ratio $S_\infty = 1.01$. Upper row shows the case with $N_d = 200$ droplets in each influence sphere of the ice crystals and droplet distance $l_0 = 5R_i$. Lower row shows the case with $N_d = 500$ and droplet distance $l_0 = 30R_i$. Note the different scaling of the axes.

even be longer if the local relaxation rate C is smaller. From the upper left panel in figure 8 we additionally observe that the red curve for ice mixing-ratio does not deviate significantly from the extreme case without local relaxation (cyan curve), until all droplets in the air parcel are evaporated (at about $t = 197\,\mathrm{s}$). Therefore, a smaller local relaxation rate increases the time until the red curve deviates from the cyan curve.

5   In the second example with a moderate droplet–ice distance $l_0 = 30R_i$, ambient saturation ratio $S_\infty = 1.01$ and $N_d = 500$ droplets, we observe similar effects as before, see lower row in figure 8. Using the larger droplet–ice distance it is important to have more droplets inside the influence spheres to compensate for the larger distance in order to observe a similar effect of the local interactions. In this case, the delay in the complete evaporation of the droplets inside the influence spheres is about $50\,\mathrm{s}$, see the lower right panel in figure 8, where the first kink is at about $t = 105\,\mathrm{s}$ and the second kink at about $t = 166\,\mathrm{s}$.

10   The longest delay of about $180\,\mathrm{s}$ in the evaporation of the droplets was found in the simulations using the small droplet–ice distance $l_0 = 5R_i$ and initial saturation ratios $S_\infty \in \{0.932, 1.01\}$ (not shown).

3.2.3   Vertical Velocity $w = 1\,\mathrm{ms}^{-1}$

For updrafts, a significant effect of local interactions on the mixing-ratios was not observed in our conducted simulations. Even in a massively water subsaturated regime $S_\infty = 0.847$ with small droplet–ice distance $l_0 = 5R_i$ and high droplet number

15    $N_d = 500$, where we expect the largest effect of the local interactions, an effect of the local interactions on the ice mixing-ratio was only minor, see the upper left panel in figure 9. Because of the ascend, the air parcel cools and the saturation ratio increases. Remarkably in this simulation, the droplets inside the influence spheres of the ice crystals managed to survive the timespan until the air parcel got saturated, whereas all droplets outside the influence spheres and in the classical treatment without the local interactions evaporated earlier, see the upper right panel in figure 9. The air parcel got saturated with respect to water at about

20    $200\,\mathrm{s}$, see figure 10. From the same figure it is evident, that the saturation ratio increased towards unrealistically high values of about $10\,\%$ after $350\,\mathrm{s}$, because we neglected activation of new droplets in our simulations. In reality, such high supersaturations are efficiently removed by activation and further diffusional growth of new droplets (Lamb and Verlinde, 2011, chapter 10).

However, considering only the simulations where the saturation ratio stayed within a reasonable realistic range, we show as an example the case with initial water supersaturation and saturation ratio $S_\infty = 1.01$, droplet distance $l_0 = 5R_i$ and $N_d = 500$

25   droplets per influence sphere. The temporal evolution of the mixing-ratios is shown in the lower row in figure 9. Compared to the classical case, the ice growth rate is slightly increased. This increase is sufficient to raise the temperature T_∞ of the air parcel by approximately $0.25\,\mathrm{K}$ over the classical case, see the left panel in figure 11. The right panel in this figure confirms that the ambient saturation ratio stayed within a realistic range. From all conducted simulations with vertical velocity $w = 1\,\mathrm{ms}^{-1}$, this was the most pronounced effect on air parcel temperature.

4   Conclusions

30   In this study, we considered the modelling of local interactions between hydrometeors, specifically the case of an ice crystal and surrounding cloud droplets. We were interested in capturing the impact of locality on the diffusional growth of the hydrom-
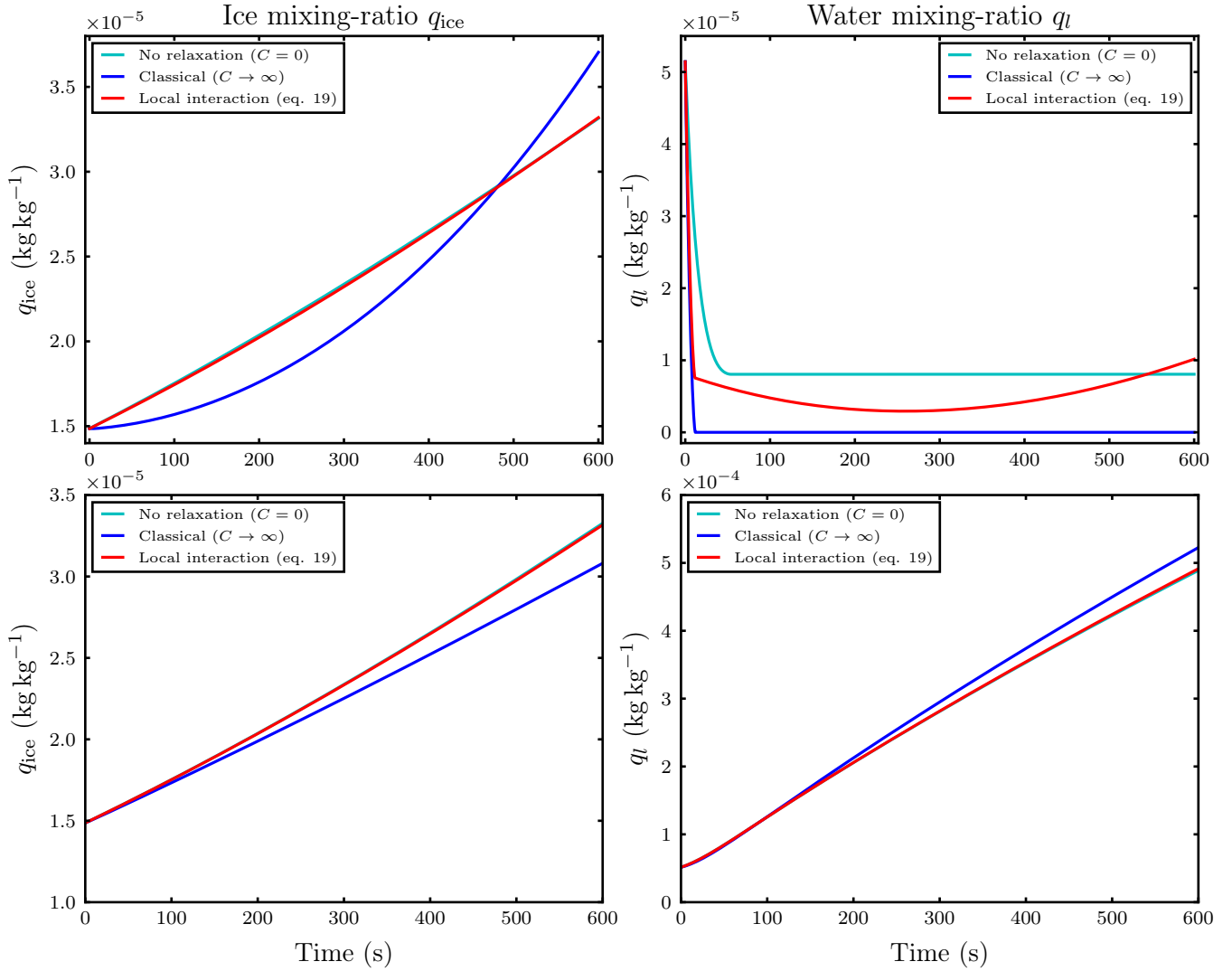
Figure 9. Temporal evolution of ice mixing-ratio (left) and liquid water mixing-ratio (right) for the parcel model simulation with $w = 1\,\mathrm{ms}^{-1}$, $N_d = 500$ droplets in each influence sphere of the ice crystals and droplet distance $l_0 = 5R_i$. Upper row is at ambient saturation ratio $S_\infty = 0.847$ and lower row at $S_\infty = 1.01$. Note the different scaling of the axes.
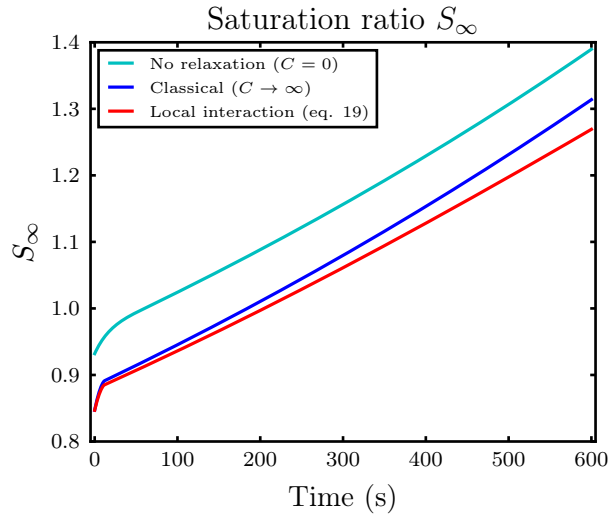
Figure 10. Temporal evolution of saturation ratio S_∞ with respect to water for the same simulation as in the upper row of figure 9 with ambient saturation ratio $S_\infty = 0.847$.
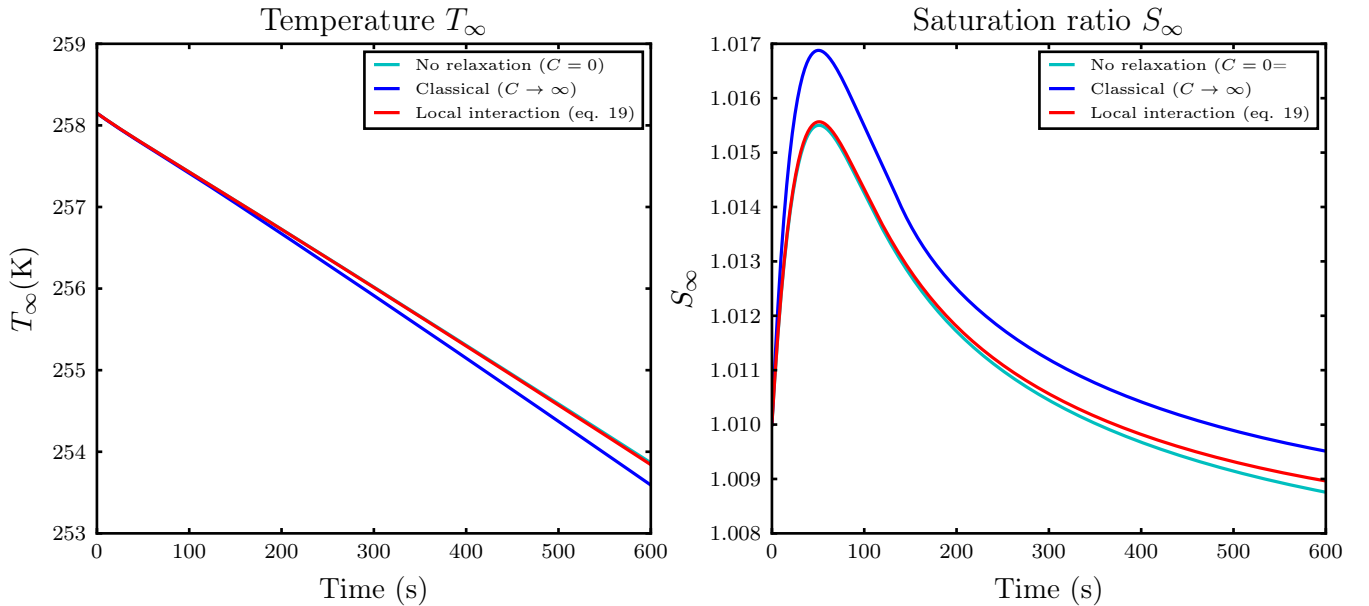
Figure 11. Temporal evolution of air parcel temperature T_∞ and saturation ratio S_∞ with respect to water for the same simulation as in the lower row in figure 9 with droplet distance $l_0 = 5R_i$.

Table 2. Summary of the observed effects within the conducted air parcel simulations.

	Stationary	Updraft	Downdraft
Parameter N_d	Increasing droplet number per ice influence sphere leads to more pronounced effects.		
Parameter l_0	Decreasing ice–droplet distance leads to more pronounced effects.		
Effect on mixing-ratios q_{ice} and q_l	Observed in water subsaturated environment	Mostly no effect, but compare the case shown in the upper row of figure 9.	Delay in the evaporation; most pronounced for initial saturation ratios $S_\infty \approx 1$ and $S_\infty > 1$.
Effect on air parcel temperature T_∞	Observed in water supersaturated environment; air parcel is warmer compared to the classical case.	Effects visible; air parcel is warmer compared to the classical case.	Not observed.

eteors. In contrast to the study by Baumgartner and Spichtinger (2017b), we suggested a formulation of the local interaction which may be suited to incorporate into a bulk microphysics model. Since this formulation allows a more physically consistent representation of the interaction between ice crystals and cloud droplets, the model may improve the representation of the Wegener-Bergeron-Findeisen process. Apart from the derivation of the model, we incorporated the suggested model into an air

5   parcel framework in order to assess the impact of local interactions on a mixed-phase cloud.

A summary of the observed effects and trends within our conducted simulations is given in table 2. The dependence on the system parameters N_d and l_0, documented in the first two rows of table 2 was to be expected by construction of the model in section 2 and is independent of the choice of the other parameters. All simulations were carried out with initial radius $R_i = 100\,\mu\text{m}$ for the ice crystal and $r_d = 10\,\mu\text{m}$ for the cloud droplets. Other choices for the initial radii will modify the rate

10   of change in mass of the hydrometeors and therefore the overall intensity and duration of local effects but not the qualitative influence of the parameters N_d and l_0.

The effect of the local interactions is primarily controlled by the droplet–ice distance and the number of droplets in the influence spheres of the ice crystals. An enhancement of the local effects on the mixing-ratios is possible through a descending air parcel being initially close to saturation or supersaturated with respect to water. This conclusion is consistent with the

15   theoretical study of Korolev (2008). In this study, various growth regimes of hydrometeors in a mixed-phase cloud were identified and connected to vertical velocities. In order to identify the different regimes, the author also employed a parcel model with monodisperse size distributions of the hydrometeors, but excluded local interactions. It was shown, that the Wegener-Bergeron-Findeisen process is only active in downdrafts and has its maximal efficiency for vertical velocities around $w =$

$0\,\mathrm{m\,s^{-1}}$. Although these findings were obtained with an idealized air parcel model, they seem to be valid in general, because similar observations were made in large-eddy simulations of real clouds (Fan et al., 2011).

The heating of the air parcel through local interactions observed in our study is due to an enhanced growth rate of the ice crystals, therefore the strength of the temperature effect additionally depends on the number of ice crystals inside the air parcel. As detailed before, the ice crystal growth rate also depends on the number N_d of droplets inside the influence spheres and the droplet–ice distance l_0. If the air parcel has a non-vanishing vertical velocity, local interactions may influence the air parcel temperature only in the case of an ascending parcel, for high droplet numbers inside the influence spheres and small droplet–ice distances.

One may speculate about the influence of a temperature change of the air parcel on its buoyancy which depends directly on the temperature of the parcel (Rogers and Yau, 1989, chapter 3). An additional heating of an air parcel with zero vertical velocity may trigger a vertical motion in an unstable stratification.

Although air parcel models are widely used, they might over- or underestimate the strength of observed effects. Therefore one should include the suggested local-interaction model into a large-eddy model framework and again analyze the influence of the local interactions seen in this study with the more realistic model, which is left for future work.

In this study we only considered local interactions regarding the diffusional growth of the ice crystal and surrounding cloud droplets. Another aspect of hydrometeors with only small distances is an enhanced collision probability. It is known that small scale turbulence enhances collision probability. In our context, an enhanced collision probability means an enhanced probability for riming of the ice crystals. In addition, the observed delays in the evaporation of the cloud droplets may also contribute to an increase in riming efficiencies.

Appendix A

In this appendix, we show an example of the effect of ice crystal shape on the diffusional growth behaviour of surrounding droplets by using the reference model described in Baumgartner and Spichtinger (2017b). The model is a direct numerical simulation model and resolves the involved hydrometeors as well as the water vapor and temperature field. We simulate a case as depicted in the schematic 2 where the ice crystal now has ellipsoidal shape with major axis length $150\,\mathrm{\mu m}$ and minor axis length $10\,\mathrm{\mu m}$. The ice crystal is placed in the center of a cubic computational domain with edge length $6000\,\mathrm{\mu m}$. We place 38 droplets with radius $10\,\mathrm{\mu m}$ along the Lebedev quadrature points (Lebedev, 1976) and distance $R_* = 600\,\mathrm{\mu m}$, matching the case $l_0 = 5R_i$ used in the air parcel simulations in subsection 3.2. The simulation time is $5\,\mathrm{s}$. Figure A1 shows contour lines of supersaturation with respect to water along a slice at height $z = 0$ through the computational domain. It is seen that the ice crystal is visible as a strong sink for water vapor, but the contour lines appear as almost spherical in some distance of the ice crystal.

Figure A2 shows the temporal evolution of the droplet masses. In the left panel, the corresponding curves of all 38 droplets are shown and a different growth behaviour is obvious. In the right panel of figure A2, only the temporal evolution of the four marked droplets in figure A1 are shown. The droplets with coordinates $(\pm 600\,\mathrm{\mu m}, 0, 0)$ are closest to the ice crystal and
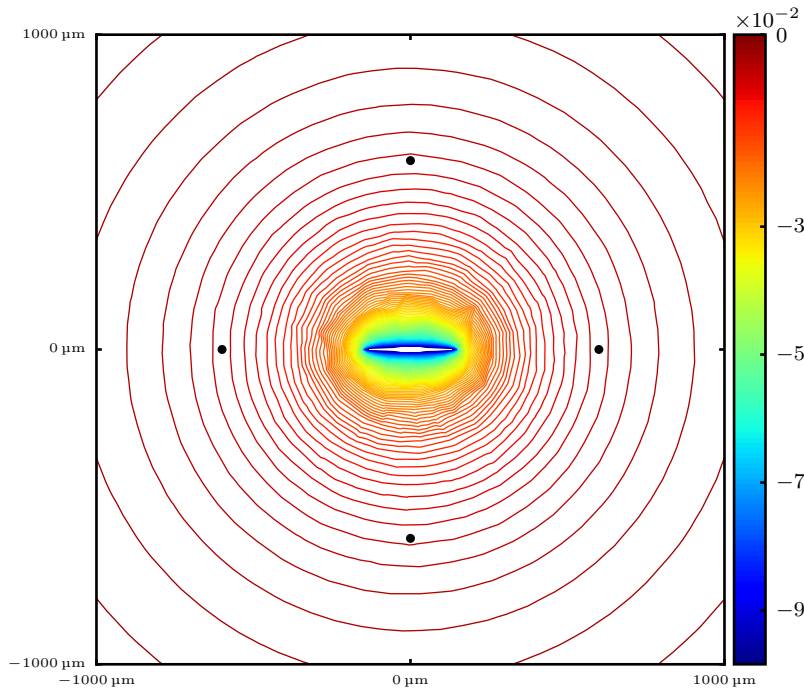
Figure A1. Contour lines of the supersaturation with respect to water around the ice crystal at time instant $5\,\mathrm{s}$. Although the computational domain is a cuboid with edge length $6000\,\mu\mathrm{m}$, the figure shows only a reduced cuboid with edge length $2000\,\mu\mathrm{m}$ centered around the ice crystal. The black dots show the positions of the droplets with coordinates $(\pm600\,\mu\mathrm{m}, 0, 0)$ and $(0, \pm600\,\mu\mathrm{m}, 0)$.

evaporate (red curves) while the droplets with coordinates $(0, \pm600\,\mu\mathrm{m}, 0)$ have largest distance from the ice crystal surface and grow (blue curves), i.e. they show different growth behaviour. According to these considerations it is obvious, that including this effect requires precise informations not only about the shape of the ice crystal but also about the relative positions of the droplets with respect to the ice crystal surface. Such informations are not available in numerical models and therefore we
5   neglect this dependence.

Appendix B

Figure B1 shows the temporal evolution of the saturation ratio $S_{\infty,i}$ with respect to ice for the first simulation in subsection 3.2.1 with vanishing velocity, $N_d = 40$ droplets per ice crystal influence sphere and droplet distance $l_0 = 5R_i$. Although the air parcel is initially subsaturated with respect to ice, the evaporating droplets release enough water vapor to the air parcel to
10   cause an ice supersaturated environment.
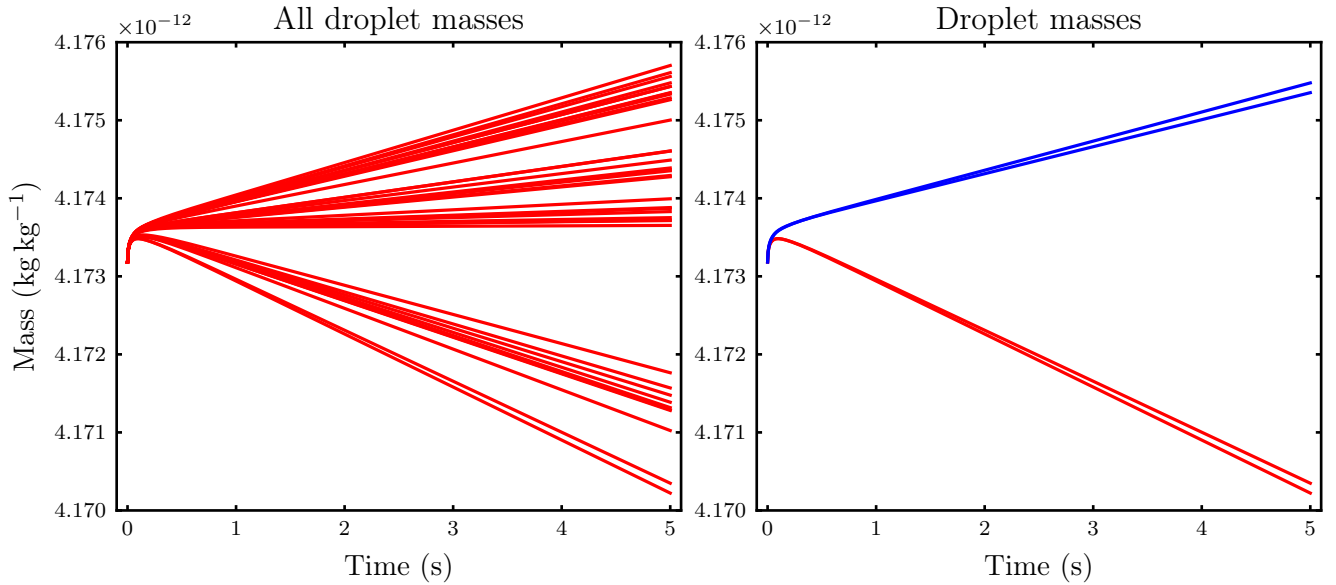
Figure A2. Temporal evolution of the droplet masses. Left panel shows the droplet masses of all 38 droplets. Right panel shows the droplet masses of the droplets with coordinates $(\pm 600\,\mu\text{m}, 0, 0)$ (red curves) and $(0, \pm 600\,\mu\text{m}, 0)$ (blue curves).
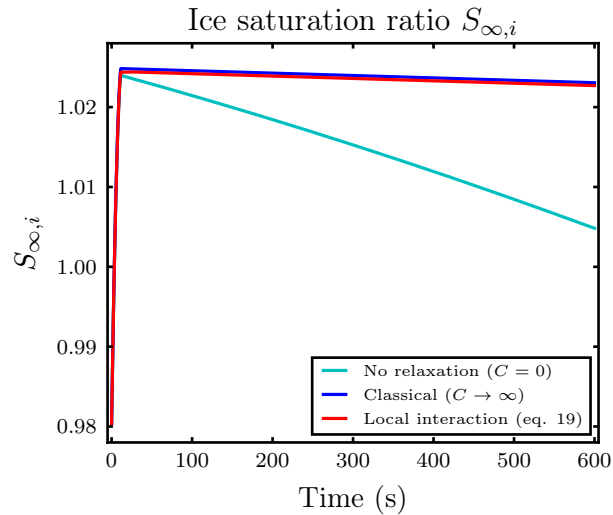
Figure B1. Temporal evolution of saturation ratio $S_{\infty, i}$ with respect to ice for the same simulation as in the upper panel in figure 6.

Acknowledgements. We thank A. Seifert for fruitful discussions. This study was prepared with support by the German "Bundesministerium für Bildung und Forschung (BMBF)" within the HD(CP)^2 initiative, project M6 (001LK1207A) and the "Deutsche Forschungsgemeinschaft (DFG)" within the project "Enabling Performance Engineering in Hesse and Rhineland-Palatinate" (grant number 320898076).

References

Baumgartner, M. and Spichtinger, P.: Diffusional growth of cloud particles: existence and uniqueness of solutions, Theoretical and Computational Fluid Dynamics, pp. 1–16, doi:10.1007/s00162-017-0437-x, 2017a.

Baumgartner, M. and Spichtinger, P.: Local Interactions by Diffusion between Mixed-Phase Hydrometeors: Insights from Model Simulations, Mathematics of Climate and Weather Forecasting, 3, 64–89, doi:10.1515/mcwf-2017-0004, 2017b.

Beals, M. J., Fugal, J. P., Shaw, R. A., Lu, J., Spuler, S. M., and Stith, J. L.: Holographic measurements of inhomogeneous cloud mixing at the centimeter scale, Science, 350, 87–90, 2015.

Bergeron, T.: The Problem of Artificial Control of Rainfall on the Globe, Tellus, 1, 32–43, 1949.

Castellano, N. E. and Avila, E. E.: Vapour density field of a population of cloud droplets, Journal of Atmospheric and Solar-Terrestrial Physics, 73, 2423–2428, 2011.

Celani, A., Falkovich, G., Mazzino, A., and Seminara, A.: Droplet condensation in turbulent flows, EPL (Europhysics Letters), 70, 775, 2005.

Celani, A., Mazzino, A., Seminara, A., and Tizzi, M.: Droplet condensation in two-dimensional Bolgiano turbulence, Journal of Turbulence, 8, N17, 2007.

Chen, J.-P. and Lamb, D.: The Theoretical Basis for the Parameterization of Ice Crystal Habits: Growth by Vapor Deposition, Journal of the Atmospheric Sciences, 51, 1206–1222, 1994.

Davis, E.: A history and state-of-the-art of accommodation coefficients, Atmospheric Research, 82, 561 – 578, 2006.

Devenish, B. J., Bartello, P., Brenguier, J.-L., Collins, L. R., Grabowski, W. W., IJzermans, R. H. A., Malinowski, S. P., Reeks, M. W., Vassilicos, J. C., Wang, L.-P., and Warhaft, Z.: Droplet growth in warm turbulent clouds, Quarterly Journal of the Royal Meteorological Society, 138, 1401–1429, 2012.

Fan, J., Ghan, S., Ovchinnikov, M., Liu, X., Rasch, P. J., and Korolev, A. V.: Representation of Arctic mixed-phase clouds and the Wegener-Bergeron-Findeisen process in climate models: Perspectives from a cloud-resolving study, Journal of Geophysical Research: Atmospheres, 116, 2011.

Findeisen, W.: Die Kolloidmeteorologischen Vorgänge bei der Niederschlagsbildung, Meteor. Z, 55, 121–133, 1938.

Fleishauer, R. P., Larson, V. E., and Haar, T. H. V.: Observed Microphysical Structure of Midlevel, Mixed-Phase Clouds, Journal of the Atmospheric Sciences, 59, 1779–1804, 2002.

Fugal, J. P. and Shaw, R. A.: Cloud particle size distributions measured with an airborne digital in-line holographic instrument, Atmospheric Measurement Techniques, 2, 259–271, 2009.

Grabowski, W. W. and Wang, L.-P.: Growth of Cloud Droplets in a Turbulent Environment, Annual Review of Fluid Mechanics, 45, 293–324, 2013.

Hobbs, P. V., Rangno, A. L., Shupe, M., and Uttal, T.: Airborne Studies of Cloud Structures over the Arctic Ocean and Comparisons with Retrievals from Ship-Based Remote Sensing Measurements, Journal of Geophysical Research: Atmospheres (1984–2012), 106, 15 029–15 044, 2001.

Korolev, A. V.: Rates of phase transformations in mixed-phase clouds, Quarterly Journal of the Royal Meteorological Society, 134, 595–608, 2008.

Korolev, A. V., Isaac, G. A., Cober, S. G., Strapp, J. W., and Hallett, J.: Microphysical characterization of mixed-phase clouds, Quarterly Journal of the Royal Meteorological Society, 129, 39–65, 2003.

Kostinski, A. B. and Shaw, R. A.: Scale-dependent droplet clustering in turbulent clouds, Journal of Fluid Mechanics, 434, 389–398, 2001.

Lamb, D. and Verlinde, J.: Physics and Chemistry of Clouds, Cambridge University Press, Cambridge, 2011.

Lebedev, V.: Quadratures on a sphere, USSR Computational Mathematics and Mathematical Physics, 16, 10 – 24, 1976.

5   Lloyd, G., Choularton, T. W., Bower, K. N., Gallagher, M. W., Connolly, P. J., Flynn, M., Farrington, R., Crosier, J., Schlenczek, O., Fugal, J., and Henneberger, J.: The origins of ice crystals measured in mixed-phase clouds at the high-alpine site Jungfraujoch, Atmospheric Chemistry and Physics, 15, 12 953–12 969, 2015.

Marshall, J. S. and Langleben, M. P.: A Theory of Snow-Crystal Habit and Growth, Journal of Meteorology, 11, 104–120, 1954.

Maxwell, J. C.: Diffusion, reprinted in W.D. Niven (Ed.), The Scientific Papers of James Clerk Maxwell, 2, 625–645, 1877.

Noh, Y.-J., Seaman, C. J., Haar, T. H. V., and Liu, G.: In Situ Aircraft Measurements of the Vertical Distribution of Liquid and Ice Water
10   Content in Midlatitude Mixed-Phase Clouds, Journal of Applied Meteorology and Climatology, 52, 269–279, 2013.

Pinto, J. O., Curry, J. A., and Intrieri, J. M.: Cloud-aerosol interactions during autumn over Beaufort Sea, Journal of Geophysical Research: Atmospheres, 106, 15 077–15 097, 2001.

Pruppacher, H. R. and Klett, J. D.: Microphysics of Clouds and Precipitation, vol. 18 of *Atmospheric and Oceanographic Sciences Library*, Kluwer Academic Publishers, Dordrecht, second revised and enlarged edition edn., 1997.

15   Reiss, H.: The Growth of Uniform Colloidal Dispersions, The Journal of Chemical Physics, 19, 482–487, 1951.

Reiss, H. and La Mer, V. K.: Diffusional Boundary Value Problems Involving Moving Boundaries, Connected with the Growth of Colloidal Particles, The Journal of Chemical Physics, 18, 1–12, 1950.

Rogers, R. and Yau, M.: A Short Course in Cloud Physics, International Series in Natural Philosophy, Butterworth-Heinemann, third edition edn., 1989.

20   Schlenczek, O., Fugal, J. P., Lloyd, G., Bower, K. N., Choularton, T. W., Flynn, M., Crosier, J., and Borrmann, S.: Microphysical Proper-ties of Ice Crystal Precipitation and Surface-Generated Ice Crystals in a High Alpine Environment in Switzerland, Journal of Applied Meteorology and Climatology, 56, 433–453, 2017.

Shaw, R. A., Reade, W. C., Collins, L. R., and Verlinde, J.: Preferential Concentration of Cloud Droplets by Turbulence: Effects on the Early Evolution of Cumulus Cloud Droplet Spectra, Journal of the Atmospheric Sciences, 55, 1965–1976, 1998.

25   Srivastava, R. C.: Growth Of Cloud Drops by Condensation: A Criticism of Currently Accepted Theory and a New Approach, Journal of the Atmospheric Sciences, 46, 869–887, 1989.

Vaillancourt, P. A. and Yau, M. K.: Review of Particle-Turbulence Interactions and Consequences for Cloud Physics, Bulletin of the American Meteorological Society, 81, 285–298, 2000.

Vaillancourt, P. A., Yau, M. K., and Grabowski, W. W.: Microscopic Approach to Cloud Droplet Growth by Condensation. Part I: Model
30   Description and Results without Turbulence, Journal of the Atmospheric Sciences, 58, 1945–1964, 2001.

Vaillancourt, P. A., Yau, M. K., Bartello, P., and Grabowski, W. W.: Microscopic Approach to Cloud Droplet Growth by Condensation. Part II: Turbulence, Clustering, and Condensational Growth, Journal of the Atmospheric Sciences, 59, 3421–3435, 2002.

Verlinde, J., Harrington, J. Y., Yannuzzi, V. T., Avramov, A., Greenberg, S., Richardson, S. J., Bahrmann, C. P., McFarquhar, G. M., Zhang, G., Johnson, N., Poellot, M. R., Mather, J. H., Turner, D. D., Eloranta, E. W., Tobin, D. C., Holz, R., Zak, B. D., Ivey, M. D., Prenni,
35   A. J., DeMott, P. J., Daniel, J. S., Kok, G. L., Sassen, K., Spangenberg, D., Minnis, P., Tooman, T. P., Shupe, M., Heymsfield, A. J., and Schofield, R.: The Mixed-Phase Arctic Cloud Experiment, Bulletin of the American Meteorological Society, 88, 205–221, 2007.

Wang, P. K.: Physics and Dynamics of Clouds and Precipitation, Cambridge University Press, Cambridge, 2013.

Wegener, A.: Thermodynamik der Atmosphäre, J. A. Barth, Leipzig, 1911.

Wood, A., Hwang, W., and Eaton, J.: Preferential concentration of particles in homogeneous and isotropic turbulence, International Journal of Multiphase Flow, 31, 1220–1230, 2005.

Zhao, Z. and Lei, H.: Aircraft observations of liquid and ice in midlatitude mixed-phase clouds, Advances in Atmospheric Sciences, 31, 604–610, 2014.